REVISION 1

Title: Magmatic volatiles and platinum-group element mineralization in the Stillwater layered intrusion, USA

Revised Word Count: 10,636 (Abstract: 351)

Authors and Affiliations: Amy P. Parker[1], Patricia L. Clay[1], Alan E. Boudreau[2], Ray Burgess[1] and Brian O'Driscoll[1*]

[1]Department of Earth and Environmental Sciences, University of Manchester, Manchester, M13 9PL, UK

[2]Division of Earth and Ocean Sciences, Nicholas School of the Environment, Duke University, Durham, NC 27708, USA

***corresponding author:** brian.odriscoll@manchester.ac.uk

For submission to the American Mineralogist Special Collection in honour of Jim Webster

Keywords: Halogen, Platinum-group elements, Stillwater intrusion, metasomatism, J-M Reef

Abstract: The activity of volatile-rich fluids may be important in the evolution of basaltic magmatic systems and associated precious metal ore formation. There is evidence for Cl-rich fluids within the Stillwater Complex (Montana, USA), which have been linked to platinum and palladium mineralisation in the economically important J-M Reef ore body. We present the first dataset for heavy halogens (Cl, Br and I) and natural noble gas isotopes in bulk rock and mineral separates from the Peridotite Zone and the Olivine-Bearing Zone I of the Stillwater Complex, including samples from the J-M Reef and G Chromitite bodies. Our data reveal concentrations of 4 to 13500 ppm for Cl, 26 ppb to 360 ppm for Br and <1 ppb to 9 ppm I over

the whole sample set. Chlorine, Br and I correlate well with each other implying a shared process and/or distribution in mineral species. Bromine/Cl and I/Cl ratios span a range from 0.3 to 35 x 10^{-3} and 5 to 900 x 10^{-6} by weight, respectively, encompassing MORB-like to more enriched compositions, particularly for Br/Cl. High Br/Cl ratios compared to MORB in some Stillwater samples suggest fractionation of halogens during the exsolution of a volatile-rich fluid, to explain the most Br-enriched samples. More generally, the presence of minerals such as scapolite, hornblende and apatite in the most halogen-enriched samples suggests that the halogen-bearing fluids were derived from cooling of the intrusion rather than late-stage (low temperature) metamorphism. The combined halogen abundance and noble gas isotope datasets imply that crustal contamination may have played a limited role in the crystallisation of pegmatoids and the G Chromitite but is not required to account for the halogen budget of the J-M Reef. High halogen contents in the sulfide-bearing J-M Reef and associated lithologies are consistent with the influence of fluid-related activity during PGE-reef formation, lending weight to the hydromagmatic model for mineralisation in the Stillwater intrusion. Our new data also imply chalcophile tendencies of Br and I over Cl in sulfides in natural systems, hinting at the importance of sulfide liquid interaction with halogen-rich fluids in the formation of sulfide-hosted precious metal ore deposits.

Introduction

Layered mafic-ultramafic intrusions represent the solidified remnants of basaltic magmatic systems (Wager and Brown, 1968; Parsons, 1987; O'Driscoll and VanTongeren, 2017). These bodies are therefore important repositories of information for the geochemical and petrological processes that operate during the solidification of magma in the Earth's crust. An abundance of evidence in layered intrusions, including within the ~2.06 Ga Bushveld Complex (South Africa; Scoates and Wall, 2015) and the ~2.71 Ga Stillwater Complex (Montana, USA; Wall et al. 2018), suggests that postcumulus processes such as recrystallisation and metasomatism of the partly-to-completely solidified crystal mush pile by late-stage volatile-rich fluids occurred

(e.g., Stumpfl, 1974; Schiffries, 1982; Stumpfl and Rucklidge, 1982; Boudreau and McCullum, 1986; Boudreau et al., 1986, Boudreau, 1999; Meurer et al., 1999; Willmore et al., 2000; McBirney, 2002; Hanley et al., 2008; Schannor et al., 2018; Su et al. 2020). The postcumulus circulation of volatile-bearing (e.g., halogen; F, Cl, Br, I) fluids may lead to the alteration of primary igneous assemblages, the formation of pegmatoidal bodies and the complexing and redistribution of base- and precious-metal species (Schiffries, 1982; Boudreau, 1999, 2016; Meurer et al., 1999; Willmore et al., 2000).

A number of layered intrusions host economic abundances of the precious metals, such as the platinum-group elements (Os, Ir, Ru, Rh, Pt and Pd; PGE). The PGE typically occur in stratiform (but not stratabound) layers referred to as ‘reefs’, and a handful of such ore bodies dominate global supply of Pt, Pd and Rh (e.g., the reefs of the Bushveld Complex account for ~75%, ~52% and ~82% of worldwide production of these metals, respectively; Mungall and Naldrett, 2008). The petrogenesis of PGE-bearing reefs has been a topic of substantial debate, traditionally dominated by two main opposing schools of thought – either mineralisation has a high temperature magmatic origin, or it occurs by late-stage metasomatic processes. The orthomagmatic models emphasise the role of sulfide in scavenging and enriching the PGE (e.g., Campbell et al., 1984), whereas the metasomatic models invoke the interaction between metal-rich fluids and near-solid cumulates. The presence of halogens, and in particular Cl, may be key for the metasomatic models, because it acts as a complexing agent for the PGE, allowing their mobilisation and redistribution into reefs (e.g., Boudreau and McCullum, 1986; Boudreau et al. 1986; Boudreau, 1999, 2016; Meurer et al. 1999; Willmore et al., 2000). However, experimental studies on the solubility of the PGE in Cl-bearing fluids appear to suggest that temperature also plays an important role here: at temperatures <500 °C Pt and Pd are not notably soluble (e.g., Gammons, 1996; Scholten et al., 2018; Bazarkina et al., 2014), whereas at temperatures >500 °C (some PGE may be extremely soluble in Cl-bearing fluids; e.g., Simon and Pettke, 2009; Tagirov et al., 2019; Simakin et al., 2021; Sullivan et al., in revision).

The primary aim of this study is to constrain the composition and provenance of late-stage magmatic fluids, with a focus on halogen geochemistry, in the Stillwater Complex (**Fig. 1**). A corollary aim is to evaluate potential links between volatiles and mineralisation by analysing PGE-enriched materials for their halogen abundances. The Stillwater Complex is an appropriate locality to carry out this work because multiple lines of evidence point toward the activity of late-stage high temperature Cl-rich fluids within the intrusion (Boudreau and McCullum, 1986; Boudreau et al. 1986; Boudreau, 1999, 2016; Meurer et al. 1999; Hanley et al., 2008). This evidence includes the occurrence of pegmatoidal bodies, which cross-cut layering throughout the intrusion and 'pothole'-like features, which are particularly evident in close proximity to the main Stillwater PGE-bearing ore body, the Johns-Manville (J-M) Reef (Boudreau, 1999). At the mineral-scale, hydrous minerals such as biotite and amphibole occur in textural equilibrium with other primary phases, and as inclusions in Cr-spinel and apatite, as well as amphibole replacing igneous pyroxene (Page and Zientek, 1987). Phases in which the halogens occur in appreciable quantities (e.g., apatite, phlogopite, amphibole) generally occur in trace abundances throughout the intrusion and are also considered to have crystallised from late-stage interstitial melts. In particular, chlorapatite compositions dominate from the G Chromitite up through to the level of the J-M Reef, with Mg-rich biotite mica and amphibole also displaying relatively unusually Cl-rich compositions in the Ultramafic Zone (Boudreau and McCullum 1986; Boudreau et al. 1986), an observation that has been used to suggest a fluid control (see also **Fig. 2**). Detailed work by Hanley et al. (2008) on fluid inclusion assemblages in lithologies below the J-M Reef supports this conclusion; the latter authors argued for the exsolution of magmatic volatiles with consequent near-solidus modification of the crystal pile in the vicinity of the ore body.

Despite the evidence for metasomatism, key questions remain about the timing and extent of volatile activity in the Stillwater Complex. This is due, in part, to the need to distinguish between the effects of high temperature metasomatism during cooling of the intrusion and a relatively late-stage low temperature (low greenschist facies) metamorphic overprint affecting

some portions of the body. More generally, there are also analytical difficulties in measuring the low-abundance halogens in the rocks that comprise most of the intrusion, in which hydrous phases are generally rare-to-absent. Here we report heavy halogen (Cl, Br and I) data from samples of pegmatoid and PGE-mineralised materials in the Ultramafic and Lower Banded Series of the Stillwater Complex, as well from massive sulfides in the footwall of the intrusion. The heavy halogens can provide powerful insights into volatile-related processes in igneous systems (Aiuppa et al. 2009). This is due to their generally incompatible nature in silicate minerals (instead preferring to enter fluid or melt phases). They are also considered to be excellent tracers for the source(s) of fluids (Schilling et al. 1980; Kendrick et al. 2014) and are fractionated during cycling between surface and biogeochemical reservoirs (e.g., the Earth's I budget is strongly dominated by organic sediments; Muramatsu and Wedepohl, 1998). Our new data comprise the first bulk rock and mineral separate Br and I measurements for the Stillwater Complex, and shed new light on the source of volatiles in the intrusion and the relationship/timing of fluid activity to sulfide-hosted PGE enrichment.

Geological Setting

The Stillwater Complex, Montana (USA; Fig. 1), is a partially-exposed layered intrusion (~42 km length and ~6 km thick; Page and Zientek, 1985) that crops out along the Beartooth uplift. A crystallisation age of 2701 ± 8 Ma (Sm-Nd; DePaolo and Wasserburg, 1979) for the Stillwater has recently been superseded by high precision U-Pb dating of zircon, baddeleyite, titanite and rutile to give a range of crystallisation ages over 2712-2709 Ma (Wall et al. 2018). The Stillwater Complex intruded a sequence of Archean (~3270 Ma; Nunes and Tilton, 1971) metasedimentary rocks (i.e., volcaniclastic shale, greywacke, breccia, quartzite and banded iron formation; Page, 1977; Labotka and Kath 2001). Sills, dikes and small bodies of massive sulfides are also present in the footwall of the complex which field observations and isotopic dating (**Fig. 2**; Premo et al. 1990) indicate are pre- to contemporaneous with intrusion of Stillwater magmas (Boudreau, 2016, and references therein). The occurrence of sulfide-bearing sills and dikes together with the massive sulfide bodies has been attributed to the

injection of sulfide-rich mafic norites or the downward migration of immiscible sulfides during crystallisation of the lowermost cumulates (Page, 1979). However recent mineralogic, geochemical and isotopic investigations have suggested that the massive sulfides are of sedimentary origin, i.e., formed from sulfide minerals in the original sedimentary protolith (e.g., Smith et al. 2017; Ripley et al. 2017). The Stillwater Complex was subsequently tilted during the Late Cretaceous Laramide Orogeny (McCallum, 1996) to its current position. Geophysical measurements indicate that the intrusion continues at depth for 25-30 km as a north-dipping, relatively flat sheet (Abbot et al., 2011), extending ~30 km to the north and ~40 km to the east (Finn et al., 2013, 2016). The Stillwater Complex is considered to have been emplaced at upper- to mid-crustal depths (Thomson, 2008; Hanley et al. 2008) and to have intruded over 50 Ma (Mogk and Mueller, 1990; Thomson, 2008) after an earlier low-pressure regional metamorphic event (525-550^{o}C and 2 kbar; Labotka and Kath, 2001). A subsequent (~1.7 Ga) low-grade regional metamorphic event produced localised greenschist facies mineral assemblages (Nunes and Tilton, 1971); however, alteration is relatively limited and the rocks retain much of their primary igneous mineralogy (e.g., **Fig. 3a**).

The stratigraphy of the Stillwater Complex is divided into three main series and consists from bottom to top of the Basal, Ultramafic and Banded Series, respectively (**Figs. 1,2**). The Basal Series comprises a lower norite (plus subsidiary anorthosite, gabbro and peridotite), grading upwards to orthopyroxenite (bronzitite; Page, 1979; McCallum, 1996). The base of the Ultramafic Series is demarcated by the first significant appearance of olivine, whilst its top boundary is placed at the first appearance of primocrystic plagioclase (McCallum, 1996). The Ultramafic Series is further subdivided into the lower Peridotite Zone (PZ) and upper Bronzitite Zone (BZ). The PZ is comprised of cyclic units (21 at Mountain View; Raedeke and McCallum, 1984) of peridotite-harzburgite-bronzitite, in which olivine ± orthopyroxene ± chromite are the major phases (McCallum, 1996). Disseminated or massive chromitite occurs in layers at the bases of many of these cyclic units (**Fig. 2**), labelled A (lowermost) to K (uppermost; Jones et al. 1960), of which the G and H seams are the thickest (>1 m thick; McCallum, 1996). Sulfides

and chlorine-rich apatite are also found in trace amounts in some of the chromitite layers (Boudreau and McCallum, 1989).

The chromitite layers are generally enriched in IPGE (i.e., iridium-group platinum-group elements; Os, Ir, Ru) that are predominantly held in platinum-group minerals such as laurite, whereas Pd and Rh are in sulfide (pentlandite, chalcopyrite and millerite) minerals (Barnes et al. 2016; Prichard et al. 2017). The major carriers of Pt are platinum-group minerals that are microstructurally associated with base-metal sulfides (Barnes et al. 2016). The E, G and H chromitites have relatively low Pt + Pd concentrations (e.g., 10 to 40 ppb for the G Chromitite) compared to the other (A, B, C, I, J, K) chromitite layers, with a collective range of 100 to 3000 ppb Pt + Pd (Zientek et al., 2002; Barnes et al., 2016). The BZ contains orthopyroxene primocrysts and is relatively uniform in appearance, with the exception of rare thin layers containing olivine ± chromite (McCallum, 1996).

Subdivisions of the Banded Series vary, but it is generally separated into the Lower Banded Series (LBS), Middle Banded Series (MBS) and Upper Banded Series (UBS) following the definitions of McCallum et al. (1980) and Raedeke and McCallum (1984). The LBS is divided into six units, of which Olivine-bearing zone I (OB-I) is host to the PGE-rich J-M-Reef (**Fig. 2**), a PGE deposit with the highest grade of Pt+Pd (~18 ppm) of all known PGE reefs (Zientek et al. 2002). The J-M Reef is generally ~2 m thick, though it may thicken in 'ballroom' structures (or at times be completely absent) from the succession. Sulfides enriched in the PGE are found in stratigraphically narrow zones in the J-M Reef and consist primarily of pyrrhotite, pentlandite and chalcopyrite, together with PGE-bearing arsenides and platinum-group minerals such as moncheite, cooperite, braggite, kotulskite and Pt-Fe alloys (McCallum, 1996; Godel and Barnes, 2008). Broadly, the PGE (except Pt) are mainly (50-80%) hosted in pentlandite and pyrrhotite, with the remainder sited in platinum-group (sulfide) minerals (Heyse, 1983; Godel and Barnes, 2008; Mansur and Barnes, 2020). Discordant pegmatoid bodies occur sporadically in the Ultramafic Series and in the Lower Banded Series below the J-M Reef and are interpreted as pods and veins of late-stage volatile-rich fluids or channel-

ways resulting from the migration of fluids through cumulates (Braun et al., 1994). The pegmatoid bodies are often mineralogically, if not texturally, identical to their host rocks (Braun et al. 1994).

The recent U-Pb geochronological study of Wall et al. (2018) proposes that the Stillwater Complex is composed of an out-of-sequence series of sub-volcanic sills intruded over a ~3 Myr interval, rather than solidifying from a single large magma chamber. In particular, the G Chromitite of the PZ is interpreted by Wall et al. to have crystallised at 2710.32 ± 0.46 Ma ($^{207}Pb/^{206}Pb$ age; 2σ), emplaced below the pre-existing Bronzitite zone; a pegmatitic feldspathic orthopyroxenite from the base of the Bronzitite Zone is dated at 2711.35 ±_0.38 Ma. The J-M Reef crystallized at ~2709 Ma (Frog Pond Adit 2709.11 ± 0.56 Ma; East Boulder Mine, 2709.28 ± 0.32 Ma; West Fork area, 2709.00 ± 0.45 Ma; Wall et al., 2018), younger than some of the overlying rocks (e.g., a MBS leucogabbro yields a $^{207}Pb/^{206}Pb$ age of 2710.44 ± 0.32). The out-of-sequence interpretation of these U-Pb ages has not gone unchallenged (Latypov, 2019).

Sample Descriptions and Analytical Techniques

Sample Descriptions

The samples studied here were selected to evaluate whether rocks that represent late-stage magmatic melts (i.e., pegmatites) and PGE-enriched rocks preserve evidence for significant halogen mobility in the Stillwater intrusion, as predicted by the hydromagmatic model for mineralisation (cf. Boudreau, 2016, and references therein). A sample of the G Chromitite layer was analysed, together with an adjacent (~1 m) pegmatoid. Two samples of the J-M Reef (from the Mountain View and Frog Pond Adit localities) were analysed, as well as two associated (stratigraphically underlying) pegmatoids. A sample of massive sulfide from the footwall of the Stillwater Complex was also analysed to elucidate the effects of localised massive sulfide formation on the halogens. Further details (sample numbers, locations,

mineralogy, petrographic information etc.) of each of the samples are provided below and in **Table S1**.

G Chromitite (ST_16_002). The G Chromitite studied here was sampled on the Mountain View Section, where Cr-spinel-rich peridotite alternates with chromitite. It contains ~30-50 vol.% Cr-spinel and ~30-55 vol.% coarse-grained olivine, with the remainder comprising plagioclase, clinopyroxene, as well as accessory amounts of biotite mica and sulfides. The Cr-spinel commonly forms a chain-texture around subhedral-euhedral olivine crystals, and the latter may contain smaller (~200 μm) inclusions of Cr-spinel (**Fig. 3a**). Intra-crystal fractures containing alteration phases (e.g., serpentine) are evident in the majority of the olivine grains. Plagioclase feldspar occurs in the interstices between olivine crystals and often encloses or is associated with Cr-spinel crystals. Minor compositional zoning is evident in plagioclase feldspar and minor secondary alteration is locally observed at plagioclase-olivine crystal boundaries.

Pegmatoid associated with G Chromitite (ST_16_003). Coarse-grained (>2 mm) orthopyroxene (bronzite) dominates (60-70 vol.%) the mineralogy of the pegmatoid associated with the G Chromitite, sampled ~1 m from ST_16_002. Orthopyroxene exhibits clinopyroxene exsolution and commonly contains inclusions of Cr-spinel, as well as minor amounts of apatite (**Fig. 3b**). Plagioclase feldspar is abundant (~15-20 vol.%) and occurs in the interstices between orthopyroxene crystals. The plagioclase exhibits compositional zoning and microstructural evidence of subsolidus strain. Clinopyroxene (~10 vol.% of sample) also occurs in interstitial areas and may completely enclose Cr-spinel crystals. Secondary amphibole locally occurs around the edges of clinopyroxene crystals. Biotite mica is present in minor proportions, associated with Cr-spinel and quartz crystals.

Sulfide-bearing J-M Reef (ST_16_004). The J-M Reef sample from the Mountain View section of the Stillwater Mine is generally coarse-grained (**Fig. 3c**) and dominated by clinopyroxene and olivine (~60 vol.%), which has been partially (or locally entirely) replaced by serpentine and chlorite. Coarse-grained sulfides, principally pentlandite and chalcopyrite

with subordinate pyrrhotite, are abundant (~30 vol.%) in this sample. The remaining ~10 vol.% comprises coarse-grained plagioclase feldspar, which is relatively unaltered, as well as minor amounts of biotite and apatite.

Sulfide-deficient J-M Reef (ST_16_008). This sample of J-M Reef material comes from near to the Frog Pond Adit area of the Stillwater Complex and is conspicuous by its lack of sulfide or any platinum-group mineral phases. Coarse-grained, euhedral, relatively unaltered plagioclase comprises ~70 vol.% of the rock, with orthopyroxene (bronzite) and clinopyroxene occurring interstitially (**Fig. 3d**). Minor amounts of oxides and alteration phases are also present.

Pegmatoid samples below sulfide-deficient J-M Reef (ST_16_009 and ST_16_011). A pegmatoidal vein (ST_16_011) sampled within ~1 m (below) of the J-M Reef (ST_16_008) consists primarily of ~1-2 mm plagioclase feldspar primocrysts (~50 vol.%), which exhibit varying degrees of alteration and in some cases compositional zoning. Orthopyroxene in most cases is cumulus (~15 vol.%, ~0.5-2 mm grainsize) and may be altered. Clinopyroxene and olivine are interstitial and commonly altered to amphibole and serpentine, respectively. Where plagioclase is in contact with serpentine (and in some cases amphibole), it displays coronas of clay minerals and talc; in some cases, the talc completely pseudomorphs the orthopyroxene (**Fig. 3e**). Other accessory alteration phases include zeolite and epidote. Another pegmatoid (ST_16_009) was sampled ~200 m below the J-M Reef (ST_16_008). The sample is characterised by extensive alteration; scapolite (~30 vol.%) has in most cases entirely replaced plagioclase feldspar (**Fig. 3f**), though some rare relict euhedral grains of the latter are still present (**Fig. 3g**). Euhedral amphibole crystals with grainsizes of ~1-4 mm comprise ~20 vol.% of the sample. Quartz (~30 vol.%) is interstitial and ranges in size from ~0.5 to 3 mm (**Fig. 3f**). The sample also contains serpentine (**Fig. 3g**) and talc, as well as oxides.

Massive sulfide (ST_16_005). This sample was collected from within the hornfels immediately below the footwall contact of the intrusion, on the Mountain View section. Sulfides

(i.e., chalcopyrite, pyrrhotite and pentlandite) form ~80-90 vol.% of the sample, with the remainder dominated by clay minerals (**Fig. 3h**).

Analytical Techniques

Electron microscopy. Chlorine and major element mapping of key samples was carried out using the Cameca SX-100 electron microprobe (EPMA) and Thermo Scientific™ Quanta™ 650 Environmental Scanning Electron Microscope (SEM) at the University of Manchester, Mapping on the EPMA was carried out using an accelerating voltage of 15 kV and a 20 nA beam current, whilst a 20 kV accelerating voltage and 6 μm spot size was employed for mapping on the SEM. EPMA maps are quantified for Cl (plus major elements including Si, Al, Na, Fe, Mg, S and P), whereas the SEM maps display relative concentrations only.

Neutron-irradiation noble gas mass spectrometry (NI-NGMS). Halogen and natural noble gas abundances were measured simultaneously utilising the neutron-irradiation noble gas mass spectrometry technique at the University of Manchester (NI-NGMS; Ruzié-Hamilton et al., 2016). Samples were first cleaned (weathered rinds removed, sanded down and cleaned with isopropanol), then coarsely-crushed and picked under a binocular microscope. In addition to bulk sample preparation, sulfide mineral separates were picked from the J-M Reef (ST_16_004), amphibole (hornblende) separates from pegmatoid ST_16_009 below the J-M Reef and orthopyroxene separates from the pegmatoid associated with the G Chromitite (ST_16_003). Approximately ~10-15 mg of each sample was then wrapped in Al foil and placed in a silica tube. Irradiation monitor minerals (scapolites BB1, BB2/SY; Kendrick 2012; Ruzié-Hamilton et al., 2016) and ^{40}Ar-^{39}Ar and I-Xe geochronology standards Hb3Gr hornblende and Shallowater enstatite (Turner et al., 1971; Brazzle et al. 1999) were distributed throughout the tube to monitor irradiation parameters (Table S2). The silica tubes were then sealed with a flame under vacuum and irradiated for 24 hours at the University of Missouri Research Reactor on the 18/04/2018. Neutron conversion [(n, γ, β reactions) resulted in the production of proxy noble gas isotopes; ^{38}Ar from Cl, $^{80,82}Kr$ from Br, and ^{128}Xe from I.

Once irradiated, the analyses were carried out over two sessions; one in November 2018 and a second set in December 2019, with a total of 3-4 replicate analyses per sample. Sample sizes for the first set of analyses were between 2-4 mg for measurement of the halogens and natural noble gases (e.g., ^{40}Ar, ^{84}Kr and ^{130}Xe) and other elements accessible by this technique (e.g., K, Ca, Ba). The focus of the second session in 2019 was exclusively on halogens, with much smaller sample sizes 0.2 mg – 2 mg to reduce sample gas release. After irradiation, samples ST_16_003, ST_16_008 and ST_16_009 and the 2019 set of ST_16_011, were separated into two components and measured separately due to sample size issues (see Table 1). The mafic portion of ST_16_003 (the G Chromitite pegmatoid) consists of orthopyroxene and biotite mica, whilst the felsic portion is predominantly plagioclase feldspar. Clinopyroxene, orthopyroxene, plus secondary serpentine and amphibole comprise the mafic portion of the S-poor J-M Reef (ST_16_008), whereas the felsic portion is dominated by plagioclase feldspar. The mafic fraction of the J-M Reef pegmatoid (ST_16_009) is principally amphibole(s) plus serpentine, whilst the felsic portion is primarily composed of quartz, plagioclase feldspar and scapolite. Sample ST_16_011 consists of a mafic portion including clinopyroxene, orthopyroxene and olivine (plus serpentine and amphibole), and a felsic portion dominated by plagioclase plus talc and clay minerals.

Samples were placed in 3 mm diameter by 5 mm deep holes drilled into an Al disk which was placed in a laser cell and heated to 120°C for 12 hours under UHV. A Cetac Fusion CO_2 laser (55 W) was employed to liberate noble gases from samples in single fusion steps, using a maximum laser output power of ~20 W with a 3 mm beam diameter. The noble gases were purified using Zr-Al getters, one of which was at room temperature and the other at 400°C, then expanded into a Thermo Scientific™ Argus VI™ static vacuum mass spectrometer. Krypton and Xe isotopes were collected in peak-hopping mode on the compact discrete dynode (CDD) electron multiplier, while five Faraday detectors and the CDD were utilised in multi-collection mode for the measurement of Ar isotopes. Air calibrations were performed daily to monitor instrument sensitivity and mass discrimination. Blank determinations were

performed every 2-3 measurements. Blank contributions for Cl and Br were typically <5%, whilst blank contributions for I were generally <13%. The noble gas isotope data were corrected for decay of ^{37}Ar and ^{39}Ar and neutron interference reactions before conversion to halogen abundances, and K parent element abundances determined from the irradiation monitor minerals (Table S2). Halogens and major elements are reported in ppb, ppm and wt%, with 1 standard error reported.

Results

Element Mapping

Element X-ray mapping reveals relative areas of Cl-enrichment in the pegmatoid samples (i.e., ST_16_003, ST_16_009), as well as the J-M Reef sample (ST_16_004), the pegmatoid vein below the J-M Reef (ST_16_011) and the massive sulfide sample (ST_16_005). No Cl-rich minerals are evident from the mapping of the G Chromitite (ST-16_002) or the sulfide-deficient J-M Reef (ST_16_008) samples. Subhedral crystals of near end-member chlorapatite (with ~6 wt% Cl) represent the main halogen-bearing phase in ST_16_003 (**Fig. 4a,b**), though accessory biotite may also contribute to the Cl budget of the rock. The pegmatoid sample (ST_16_009) associated with the J-M Reef hosts minor amounts of Cl-bearing apatite; however, most Cl appears to be hosted in phases associated with alteration of plagioclase feldspar (e.g., scapolite; **Fig. 4c, Fig. S.1**), as well as amphibole and serpentine. Scapolite is the bulk Cl-carrier in ST_16_009 and appears to be intermediate, between the meionite and marialite end-members, in composition (**Fig. 4d**). Sample ST_16_009 exhibits at least two populations of amphibole; magnesio-hornblende, which is the dominant amphibole phase, and ferro-hornblende. The ferro-hornblende appears to replace the magnesio-hornblende and is slightly more Cl-enriched (**Fig. 4c, Fig. S.1**). The J-M Reef sample (ST_16_004; **Fig. 4e**) contains apatite, which has a lower Cl abundance (i.e., ~3 wt% Cl) compared to the G Chromitite pegmatoid apatite. Chlorine-bearing alteration phases (e.g., serpentine) and veins cross-cutting the primary mineral assemblage are also observed in the J-M Reef sample ST_16_004; these are not as Cl-rich as the apatite and some also display Fe enrichment (**Fig.**

345 **4f**). Alteration phases (veins and primocryst coronas of serpentine and talc) appear to be
346 relatively enriched in Cl in the pegmatoid sample ST_16_011 (**Fig. 4g**). Evidence for modest
347 Cl-enrichment is present in the clay minerals of the massive sulfide sample (ST_16_005; **Fig.**
348 **4h**).

349 **Heavy Halogen Abundances in the Stillwater Complex**

350 The halogen abundance and ratio data of individual and replicate samples of the Stillwater
351 Complex are presented in Table 1 and in **Figure 5**. Inter-sample variability, representing the
352 natural heterogeneity within samples, can be high between mafic and felsic portions of the
353 same sample (i.e., up to ~2 orders of magnitude). In general, variation is highest within the
354 bulk pegmatoid (ST_16_009) and bulk J-M Reef (ST_16_004) samples. Variation between
355 mineral separates is generally low, particularly for Br and I, but varies by up to a factor of 5 for
356 Cl abundances. Overall, halogen concentrations range from 4 to 13500 ppm for Cl, 26 ppb to
357 360 ppm for Br and <1 ppb to 9 ppm for all samples analysed. Well-developed positive
358 correlations are observed between samples for Br versus Cl and I versus Cl and (**Fig. 5**).
359 Bromine and Cl values define an array lying above the seawater reference ratio line (**Fig. 5a**),
360 whilst in I versus Cl space, the sample array lies above that of the seawater line and just below
361 or on that of the MORB line (**Fig. 5b**). The J-M Reef samples and the associated pegmatoid
362 vein (ST_16_004, ST_16_008 and ST_16_011, respectively) are grouped between the
363 seawater and MORB reference ratio lines.

364 Halogens in bulk rock samples from the J-M Reef (ST_16_004 and ST_16_008; n = 4 and n
365 = 3, respectively) span a range of 6 – 641 ppm Cl, 103 – 6420 ppb Br and 0.6 – 29.1 ppb I.
366 Halogen concentrations are systematically lower in the sulfide-deficient J-M Reef sample (**Fig.**
367 **5**), with maximum concentrations of 346 ppm, 763 ppb and 9 ppb for Cl, Br and I, respectively
368 (Table 1). For ST_16_008, the plagioclase-dominant felsic fraction reveals consistently lower
369 halogen concentrations of 36 - 45 ppm Cl, 103 - 359 ppb Br, and 0.6 – 4.4 ppb I, than the
370 mafic (pyroxene plus secondary amphibole and serpentine) component which has 47 - 346
371 ppm, 213 - 763 ppb and 3 - 9 ppb Cl, Br and I, respectively. In the sulfide separate (n = 4)

372 from ST_16_004, halogen concentrations are generally lower than the J-M Reef bulk rock
373 measurements, with maximum concentrations of 50 ppm Cl, 617 ppb Br and 5.9 ppb I, but
374 more enriched than the plagioclase (felsic) component of ST_16_008.

375 The pegmatoid from below the J-M Reef (ST_16_009, n = 6) displays the highest halogen
376 contents of all samples studied here (by an order of magnitude; Table 1 and **Fig. 5**). Chlorine
377 appears to be more enriched in the mafic component of the sample, with 2830 – 13500 ppm
378 Cl, compared to 169 – 10100 ppm in the felsic component (the latter comprising scapolite,
379 plagioclase and quartz). The felsic component displays the highest I and Br abundances, with
380 360 ppm Br and 9.2 ppm I. However, the overall concentrations of halogens are broadly similar
381 between the two components (Table 1). Amphibole separates from ST_16_009 (n = 3) exhibit
382 maximum Cl concentrations of 3030 ppm and significantly lower (than bulk rock) Br and I
383 contents of 620 – 820 ppb and 16.5 – 17.9 ppb, respectively (**Fig. 5**). The pegmatoid vein
384 sample (ST_16_011, n = 4) also reveals relatively high halogen concentrations (maximum 871
385 ppm Cl, 6.6 ppm Br and 33.5 ppb I), particularly compared to the adjacent J-M Reef sample
386 (ST_16_008; **Fig. 5**). The mafic separates from ST_16_011 are enriched by at least an order
387 of magnitude in Cl, Br and I compared to the felsic phases (**Table 1**). The pegmatoid
388 associated with the G Chromitite (ST_16_003, n = 3) has relatively low halogen contents of 6
389 – 76 ppm Cl, 46 – 780 ppb Br and 1.9 – 15.3 ppb I, compared to ST_16_009. The mafic
390 component of ST_16_003 has concentrations of 627 - 780 ppb Br, which is notably higher
391 than the felsic component (with concentrations of 46 - 248 ppb Br; **Table 1**) for this sample.
392 Orthopyroxene separates from ST_16_003 (n = 3) exhibit halogen concentrations of 26 - 76
393 ppm Cl, 107 - 334 ppb Br and 10.9 – 15.3 ppb I, with slightly higher Cl and I contents overall
394 than indicated by the bulk measurements (**Fig. 5**). The G Chromitite (ST_16_002, n = 4) bulk
395 sample has maximum concentrations of 105 ppm Cl, 1.6 ppm Br, and 13.2 ppb I. This Br value
396 is significantly higher than that of the associated pegmatoid (ST_16_003; **Fig. 5**).

The massive sulfides from the Stillwater contact zone (ST_16_005, n = 4) exhibit relatively low halogen concentrations compared to the Stillwater intrusion samples, of 4 - 27 ppm Cl, 26 - 186 ppb Br and 0.7 – 1.9 ppb I (**Table 1**, **Fig. 5**).

Noble Gas Isotope Systematics

The natural noble gases were measured concurrently with noble gases produced from neutron irradiation; the data are presented in **Table S2** and **Figure 6**. Noble gas isotopes are also a useful diagnostic tool to assess the provenance of fluids, particularly the $^{130}Xe/^{36}Ar$ and $^{84}Kr/^{36}Ar$ ratios, which complement the halogen measurements well as their compositions for air, MORB, seawater and sedimentary reservoirs are well-characterised (Matsuda and Nagano, 1986; Staudacher and Allègre, 1988; Moreira et al., 1998; Holland and Ballentine, 2006; Kendrick et al., 2013). The 2018 set of analyses yielded data with low enough uncertainties to allow meaningful comparisons to be made with these reservoirs (**Fig. 6, Table S2**). Overall, the Stillwater samples span an area in $^{130}Xe/^{36}Ar$ and $^{84}Kr/^{36}Ar$ space from MORB-like values for each ratio (MORB: $^{84}Kr/^{36}Ar$ =0.05, $^{130}Xe/^{36}Ar \sim 1 \times 10^{-3}$; Moreira et al., 1998; Holland and Ballentine, 2006) to the marine sedimentary field (i.e., with a range of $^{84}Kr/^{36}Ar$ =0.1–0.2 and $^{130}Xe/^{36}Ar$ =2–3 $\times 10^{-3}$; Matsuda and Nagano, 1986; Staudacher and Allègre, 1988). The G Chromitite pegmatoid orthopyroxene separate (ST_16_003) exhibits the highest $^{130}Xe/^{36}Ar$ ratios of 2.6 $\times 10^{-3}$ to 4.7 $\times 10^{-3}$. The J-M Reef samples (ST_16_004 and ST_16_008) and associated pegmatoids (ST_16_009 and ST_16_011) plus the massive sulfides (ST_16_005) appear to cluster slightly closer to the MORB value (i.e., do not extend far into the sedimentary field in $^{130}Xe/^{36}Ar$ space).

Discussion

The new halogen data from the Stillwater Complex point towards the existence of halogen-enriched fluids during the evolution of the intrusion, in agreement with previous studies (e.g., Boudreau et al., 1986; Hanley et al., 2008, Boudreau, 2016). High-Cl contents for Stillwater lithologies, ranging up to 13500 ppm in pegmatoid ST_16_009, suggest the addition and/or

enrichment of Cl in the Stillwater magmatic system. This is because most mafic silicate melts contain a maximum of 0.5-1.0 wt.% Cl (Webster et al., 1999). The behaviour of Br and I provides insight into the provenance and evolution of halogen-bearing fluids in the intrusion. In particular, halogen ratios of Br/Cl and I/Cl may be utilised to discriminate between various fluid reservoirs (**Fig. 5**; e.g., White et al. 1963; Collins and Egleson, 1967; Carpenter, 1978; Bohlke and Irwin, 1992; Muramatsu and Wedepohl, 1998; Kendrick et al. 2014). Iodine/Cl ratios for the Stillwater Complex range from close to established MORB values ($60 \pm 30 \times 10^{-6}$ wt. I/Cl; Kendrick et al., 2012a; 2013; 2014) to slightly more enriched I/Cl (5 ± 1 to $900 \pm 331 \times 10^{-6}$ wt. I/Cl; **Fig. 5c**). Bromine/Cl ratios exhibit variation from MORB-like ($2.86 \pm 0.6 \times 10^{-3}$ wt.; Kendrick et al., 2012; 2013; 2014) to highly-enriched values, with a maximum of $35.3 \pm 0.1 \times 10^{-3}$ wt. for the J-M Reef pegmatoid (ST_16_009; **Fig. 5**). Overall, the Stillwater halogens correlate positively with one another (**Fig. 5a,b**), which suggests some commonality in the mineral phases hosting them in the different samples, or possibly a single fluid source and/or similar partitioning behaviour within the intrusion.

Evaluating the Effects of Late-Stage Metamorphism on Halogen Budgets

The hydromagmatic model for PGE mineralisation in the Stillwater intrusion invokes the presence of relatively high temperature (>>500 ^{o}C) fluids derived from cooling of the magma body. In order to fully evaluate halogen behaviour in this context, it is important to first assess the possible effects of subsequent low temperature alteration by non-magmatic (metamorphic) fluids. Field, textural, geochemical and isotopic studies have attributed recrystallisation, localised ore-tenor downgrading and alteration of host rock compositions to low temperature (<400 ^{o}C) fluid activity during lower greenschist-facies metamorphism of the Stillwater intrusion at ~1700-1600 Ma (Nunes and Tilton, 1971; Page, 1976, 1977; McCallum et al., 1980; 1999; Boudreau and McCallum, 1990; Czamanske and Loferski, 1996; Lechler et al. 2002; Polovina et al. 2004). In the materials studied here, hydrothermal alteration is evident in those samples associated with the J-M Reef, manifested by fractures associated with semi-pervasive alteration of primary igneous assemblages to Ca-Mg-hydroxysilicates (**Fig. 2c**;

Volborth et al. 1986; McCallum et al. 1980; 1999; Czamanske and Loferski, 1996; Polovina et al. 2004). Sample ST_16_004 exhibits microstructural alteration characteristic of the J-M Reef (**Figs. 2c, 3d,e**) with moderately halogen- and Fe-rich veins cross-cutting primary igneous minerals; some of these veins appear to be linked to the partial serpentinization of the sample. The pegmatoids associated with the J-M Reef (ST_16_009 and ST_16_011, respectively) also exhibit extensive alteration (e.g., serpentine, talc, alteration coronas).

Hanley et al. (2008) reported fluid inclusions in Stillwater rocks that preserve evidence for both magmatic and metamorphic fluid activity. In particular, these authors made a detailed study of a pegmatoidal body in Gabbronorite I of the LBS and, in addition to a suite of high temperature halide melt and brines (discussed below), they observed late-stage secondary inclusions containing regional metamorphic fluids hosted in quartz. The secondary inclusions recorded $CaCl_2$-$MgCl_2$-H_2O solutions of low to moderate salinity and trapping conditions between 125 and 225^{o}C, at zeolite facies conditions. The fluids therefore cooled before entrapment and were attributed by Hanley et al. (2008) to the ~1.7 Ga metamorphic event. Hanley et al. (2008) suggested that these fluids became somewhat enriched in Cl due to the consumption of H_2O (and exclusion of Cl) during the formation of hydroxysilicates (e.g., chlorite). As the temperature decreased during the waning stages of metamorphism to zeolite-facies conditions, the fluids may therefore have concentrated dissolved salts (Hanley et al., 2008).

Although low temperature metamorphism may have affected rocks that had already experienced high temperature metasomatism, multiple lines of evidence suggest that the halogen budgets of the samples studied here are not a consequence of the former. For example, element mapping shows that apatite hosts the most significant halogen concentrations in ST_16_004 (**Fig. 4e**), but as apatite is cross-cut by the Fe-rich veins it is most likely to pre-date the low temperature serpentinization event (see also Boudreau et al., 1986). In addition, in ST_16_009, which contains the highest abundances of halogens in our dataset, amphibole and particularly scapolite are the main Cl carriers in the sample. It is unlikely that lower greenschist facies metamorphism would provide sufficient temperature to

cause scapolisation of plagioclase feldspar and amphibole crystallisation (**Fig. 3c,d,f, Fig. S.1**), as observed in this sample. Indeed, scapolisation of plagioclase feldspar has been attributed to the infiltration of NaCl fluids at 600-700^{o}C in metagabbros of the Bamble Lithotectonic Domain, South Norway (Engvik et al., 2011, 2018). We note that ST_16_005, which contains some clay minerals, has a noble gas isotope (and halogen) composition similar to the samples from the intrusion, suggesting that low temperature alteration has not affected its volatile geochemistry, e.g., by imparting an air-like signature (**Fig. 6a**). Finally, given that there is no systematic difference in Br/Cl and I/Cl ratios (**Fig. 5**) between relatively altered samples (e.g., ST_16_009, ST_16_011) and samples with little to no alteration (e.g., ST_16_002, ST_16_008), fluids associated with the metamorphic event at ~1700-1600 Ma are not considered to have significantly mobilised or otherwise fractionated the halogen systematics of the samples studied, and the data can be interpreted in the context of high temperature metasomatic processes.

Mineralogical Controls on Halogen Distributions

The pegmatoids (ST_16_009 and ST_16_011) associated with the Frog Pond Adit J-M Reef locality are the most halogen-enriched samples analyzed in this study. In ST_16_009, most of the Cl is hosted in hydrous phases such as scapolite and amphibole. In ST_16_11, the heavy halogens are concentrated mainly in the mafic separates analysed and serpentine shows some Cl enrichment, but on the basis of the bulk rock concentrations we suggest that any low temperature halogen mobilisation in this sample has been localised. (**Fig. 4c,d**). Given the relatively similar partitioning behaviour of the halogens (e.g., **Fig. 5a,b**), we assume that Br and I are also concentrated in or associated with the phases above. The felsic portion of ST_16_009 exhibits the higher Br and I enrichments (359 ppm Br and 9.2 ppm I) compared to the mafic portion; however, the highest Cl contents are recorded in the latter portion (13500 ppm), which is dominantly comprised of amphibole. The amphibole separate for ST_16_009 displays preferential Cl-enrichment over Br and I (as might be expected from experimental partitioning behavior; e.g., Svensen et al. 2001; Kendrick et al. 2013; **Fig. 5**), which follows

the relative Cl-enrichment observed in the mafic fraction over the felsic fraction seen in this sample. However, at least two generations of amphibole are evident in this sample based on petrographic observation (**Fig. 4c, Fig. S.1**). The magnesium-hornblende appears to be earlier-formed but is Cl-poor compared to the ferro-hornblende, which exhibits relative Cl-enrichment, fitting what is known about Cl partitioning into Mg end-member amphibole (and biotite; Volfinger et al. 1985).

The mafic portion of the G Chromitite pegmatoid (ST_16_003) exhibits higher overall halogen contents than the felsic fraction (i.e., 627 – 780 ppb Br compared to 46 – 248 ppb Br, respectively; **Table 1**), highlighting the influence of phases such as biotite and amphibole on the distribution of halogens in this sample. Element mapping indicates that the Cl budget of ST_16_003 is also influenced by chlorapatite, which commonly occurs as inclusions in orthopyroxene (**Fig. 4a,b**). Chlorine enrichment is also apparent in apatite from the J-M Reef sample and the pegmatoid below the J-M Reef (ST_16_004 and ST_16_009 respectively; **Fig. 4d,e**). Apatite is therefore a key halogen-bearing mineral in several of the Stillwater lithologies; for example, a simple mass balance calculation indicates that ~0.3-0.5 vol% of chlorapatite could account entirely for the quantities of Cl and Br measured by NI-NGMS in ST_16_004. Similarly, for the G Chromitite pegmatoid (ST_16_003), maximum Cl and Br concentrations of 44 ppm and 545 ppb are consistent with chlorapatite abundances of <0.1 vol%.

The highest Cl and Br concentrations in the J-M Reef pegmatoid (ST_16_009) require unrealistic quantities of apatite (8-20 vol%) to account for the measured Cl and Br contents. This quantity of apatite is not observed in ST_16_009; however, Cl is also contained in alteration phases (e.g., serpentine, scapolite, amphiboles; **Fig. 3d**) in this sample. The similarity in halogen contents and ratios between the mafic and felsic components points towards relatively equal distributions between the two fractions; a combination of phases such as amphibole, scapolite and apatite are therefore likely to be the main hosts for the halogens here. The relatively low halogen concentrations of the sulfide-deficient J-M Reef (ST_16_008) or G Chromitite (ST_16_002) compared to the sulfide-rich J-M Reef and associated

pegmatoids may be explained by minor (~0.1 vol%) apatite. No hydrous phases were observed in these samples (with the exception of minor amounts – maximum 0.5 vol% – of alteration phases).

Although we did not make a detailed study of fluid inclusions in our samples, we note that Hanley et al. (2008) report halide melt and hydrosaline inclusions in quartz from a pegmatite in the LBS. In that context, it is interesting to note that the felsic component of ST_16_009 is relatively enriched in Br and I compared to Cl, and we cannot rule out that fluid inclusions host at least some of the halogens in this and other pegmatoids studied here. However, the fractionation of Cl from Br and I suggests that crystallisation of amphibole in the pegmatite also played a part in controlling the distribution of volatiles in these rocks (see below).

Constraints on the fluid composition(s) and provenance

An external (crustal) source for the halogens? Hydrous minerals in equilibrium with a silicate melt acquire low Cl/F ratios; e.g., the anion preference of apatite is F>OH>>Cl (Stormer and Carmichael, 1971; Korzhinskiy, 1982; Kusebauch et al. 2015). Based on the Cl and F contents of natural apatite and associated glass reported by Piccoli and Candela (1994) for the Bishop Tuff and Tuolumne intrusive suite, the Stillwater parental magmas are considered to have had Cl contents ~2 orders of magnitude greater than their F concentrations to produce the interstitial chlorapatite in rocks underlying OB-I in the Stillwater intrusion (**Fig. 2**; Boudreau et al., 1997). The source of the high-Cl content of volatiles in the Stillwater intrusion has been problematic to resolve; the anomalously high and variable Cl/F ratios observed in hydrous minerals in the intrusion have led to a debate over the addition of Cl from external sources versus a high-Cl parental magma to the Stillwater intrusion (Boudreau and Meurer, 1999; Willmore et al. 2000; Willmore et al. 2002). On the one hand, Boudreau et al. (1997) reported crustal-like signatures in $\delta^{37}Cl$ isotope measurements from biotite in the Ultramafic Series and the J-M Reef (ranging from 0.27‰ to -0.93‰). Alternatively, boninitic parental magma (i.e., sourced from metasomatized depleted mantle), has been proposed to explain the high-Cl content of the Stillwater intrusion, with further processes such as limited crustal contamination

and volatile-refining acting to further enrich Cl-contents in fluids within the intrusion (Boudreau et al. 1997; Boudreau, 2016).

A recent study of heavy halogens in the Rum layered intrusion (NW Scotland) attributed relatively high iodine concentrations and I/Cl ratios in the Rum cumulates to crustal contamination (Parker et al. 2019). Iodine may act as a sensitive indicator of contamination by organic-bearing sediments due to its biophilic behaviour (Li and Schoomaker, 2003; Muramatsu and Wedepohl, 1998; Kendrick et al. 2017). The Rum intrusion samples span I/Cl ratios from MORB to higher values characteristic of sediments (**Fig. 5**), with I concentrations between 1 and 363 ppb. By comparison, the Stillwater intrusion displays more limited I enrichment, generally falling in a range between 0.6 - 33.5 ppb. The exception is the J-M Reef pegmatoid sample (ST_16_009) with elevated I concentrations of up to 9.2 ppm. Despite these generally low I contents, Stillwater I/Cl ratios span a range from MORB/mantle-like (Kendrick et al. 2012a; 2013; 2014) to more enriched ratios akin to sedimentary values (**Fig. 5c**). The pegmatoids (ST_16_003 and ST_16_009) in particular display elevated I/Cl ratios, whereas the G Chromitite (ST_16_002) has somewhat elevated I/Cl compared to MORB. The I/Cl ratios of the J-M Reef samples (ST_16_004 and ST_16_008), plus associated pegmatoid vein material (ST_16_011), are approximately an order of magnitude lower than the pegmatoids ST_16_003 and ST_19_009. The massive sulfides exhibit I/Cl ratios similar to the G Chromitite.

The overall range in I/Cl ratios might be taken to suggest some limited crustal contamination of the Stillwater magmas, as proposed previously (e.g., Wooden et al., 1991; Horan et al. 2001; Spandler et al. 2005; Ripley et al. 2017). Noble gas ratios of $^{84}Kr/^{36}Ar$ and $^{130}Xe/^{36}Ar$ range between MORB and the marine sediment field ($^{130}Xe/^{36}Ar = 2.5 \times 10^{-3}$ and $^{130}Xe/^{36}Ar = 1.3 \times 10^{-3}$ respectively) for the majority of samples. The G Chromitite (ST_16_002) and associated pegmatoid (ST_16_003) have the highest values (1.9×10^{-3} and 2.6×10^{-3} to 4.7×10^{-3} respectively) that range into the marine sediment field for $^{130}Xe/^{36}Ar$, suggesting that these samples may have experienced a greater degree of crustal contamination, similar to that

585 observed in the noble gas isotope ratios of the Rum layered intrusion rocks (**Fig. 6**). This trend
586 is somewhat supported by $I/^{36}Ar$ and $^{130}Xe/^{36}Ar$ (**Fig. 6b** and Table S2), which shows that the
587 G Chromitite and associated pegmatoid (ST_16_002 and ST_16_003, respectively) and the
588 J-M Reef pegmatoids (ST_16_009 and ST_16_011) range towards the highest $I/^{36}Ar$ and
589 $^{130}Xe/^{36}Ar$ values, pointing towards addition of a sedimentary component.

590 Based upon $\delta^{34}S$ and $\Delta^{33}S$ analyses of the rocks of the Basal Series, which range from -0.9
591 to +3.0‰ ($\delta^{34}S$) and +0.01 to +0.18‰ ($\Delta^{33}S$), Ripley et al. (2017) argued for significant
592 magma-crust interaction at this level of the intrusion. Indeed, Ripley et al. (2017) estimated
593 that ~50% of the S in some samples was of crustal origin. The latter authors measured $\delta^{34}S$
594 of +8.2‰ in the G Chromitite, suggesting a contribution of crustally-derived S, in contrast with
595 the A, B and C Chromitites which mostly fell in the $\delta^{34}S$ range of -0.6 to +0.7‰ (more
596 consistent with mantle-derived S). The J-M Reef samples analysed by Ripley et al. (2017)
597 define a range of -1.3 to +1.8‰ $\delta^{34}S$ and -0.06 to +0.06‰ $\Delta^{33}S$, suggesting that either crustal
598 contamination was relatively insignificant for the reef and associated PGE enrichment or that
599 any contaminants involved had $\delta^{34}S$ not distinguishable from accepted mantle values. Given
600 the evidence from other isotopic systems (e.g., $^{143}Nd/^{144}Nd$ and $^{187}Os/^{188}Os$) that preserve
601 evidence for an Archean crustal component in J-M Reef rocks (Lambert et al., 1994), the latter
602 scenario is more likely. However, our new halogen data mimic the behaviour of the sulfur
603 isotopes in that the I/Cl enrichments above MORB values for the G Chromitite and pegmatoid
604 samples are permissive of them carrying a crustal I signature, whereas the lower I/Cl values
605 for the J-M Reef materials do not preserve such evidence.

606 A plausible local source of I enrichment to the Stillwater magma chamber is the footwall
607 hornfels material, considered to have had marine shale and greywacke protoliths, with a mafic
608 volcanogenic component (Page and Zientek, 1985). Ripley et al. (2017) considered the
609 hornfels as a potential contaminant of the Stillwater magmas, and found these rocks could be
610 grouped into populations on the basis of S isotopes. One population has $\delta^{34}S$ and $\Delta^{33}S$ values
611 from 0 to -1.4‰ and +0.06 to +0.32‰, respectively, whereas the second population is

characterised by $\delta^{34}S$ of +1.5 to +3.6‰ and $\Delta^{33}S$ values from +0.01 to -0.23‰. Ripley et al. (2017) noted that it would require selective contamination by only one hornfels population, which seems unlikely. Whilst it is reasonable to assume that the protolith of the hornfels may have contained appreciable I contents (e.g., up to 30 ± 15 ppm I for marine shales; Kendrick et al., 2017), it is also possible that dehydration caused by pre-Stillwater metamorphism and/or Stillwater intrusion itself could have resulted in halogen loss from the country rocks, though such behaviour is not well constrained (Boneß et al., 1991; Hanley and Koga, 2018). It is also possible that the hornfels protolith was not I-rich, but more of a volcaniclastic greywacke (Page, 1977), such that the original I contents were much lower than the values above (100s ppb; Boneß et al., 1991). Sample ST_16_005 was analysed here to assess the effect of massive sulfide formation on the halogens, given the suggestion that they could have formed from fluids associated with dehydration of the Stillwater country rocks that had mobilised crustal sulfur (Boudreau et al., 2021, and references therein). Despite the relatively low I abundances measured in the massive sulfide (0.7 – 1.9 ppb), it is worth noting that the I/Cl ratio of ST_16_005 lies toward the enriched end (close to the enriched I/Cl pegmatoids and G Chromitite samples) of the array in **Figure 5c**, lending some qualitative weight that the sulfides formed from similar fluids to those that formed ST_16_002. In summary, our new halogen data (particularly the I/Cl ratios and noble gas isotopes) do lend some support to the suggestions of previous workers that the Stillwater intrusion records evidence of limited but locally variable amounts of contamination by crustal fluids.

Relationship of Br/Cl and fluid activity. One of the most notable features of the Stillwater halogen data is the range from MORB-like to more enriched Br/Cl ratios (**Fig. 5c**). High Br/Cl values are particularly evident in the bulk rock fractions of the pegmatoid ST_16_009. As noted earlier, Br and Cl (and I) contents correlate well across all sample types, suggesting a broadly similar control (i.e., processes or mineralogical controls) on the distribution of all of the heavy halogens. Chlorine, Br and I are highly-incompatible elements in most silicate minerals ($D_{halogen}^{mineral/melt}$<<1) and should thus behave similarly during progressive crystallisation of

639 magma (Parker et al., 2019). Studies on basaltic glasses have shown that halogens are not
640 fractionated from each other by melting or crystallisation processes at high temperatures
641 (Schilling et al., 1980, Kendrick et al., 2012b); therefore, processes associated with magmatic
642 fractionation are unlikely to influence the halogen ratios observed in the Stillwater Complex.
643 The relatively high Br/Cl ratios are not likely the result of Br addition, as there is no known
644 reservoir enriched in Br over Cl (Hanley and Koga, 2018), and are thus more likely the result
645 of a process involving Cl-loss.

646 Several processes have been proposed to be capable of modifying Br/Cl ratios, including
647 selective incorporation of Cl into minerals (e.g., halite, amphibole; Braitsch, 1971; Kendrick et
648 al., 2013), or density-dependent differential partitioning (Oosting and Von Damm, 1996; Berndt
649 and Seyfried, 1997; Von Damm et al., 2003). The latter process fractionates Cl and Br during
650 vapor–brine separation and phase segregation (e.g., Berndt and Seyfried, 1997; Liebscher et
651 al., 2006). A key process advocated in the enrichment of volatiles in the Stillwater Complex
652 is 'fluid fluxing' or 'volatile-refining' (Boudreau, 1988; 1999; 2016; Willmore et al. 2000; Hanley
653 et al. 2008). This process is based upon the exsolution and migration of a volatile-rich fluid
654 from solidified/near-solidified cumulates. As the cumulate pile degasses during cooling and
655 crystallisation, this fluid mobilises and migrates upwards, enriching the intercumulus liquids as
656 the crystal pile grows. Sulfur is highly soluble in hydrosaline volatiles (Ulrich et al., 2001);
657 consequently, sulfide minerals are resorbed in the cumulate pile. Once this fluid migrates to
658 hotter, fluid-undersaturated intercumulus liquids, sulfide precipitation is induced, with
659 important consequences for PGE-mineralisation (see below; Boudreau and McCallum, 1992;
660 Boudreau, 1999, 2016). This hydromagmatic model has been likened to slab dehydration and
661 subsequent hydration melting of the overlying mantle wedge during subduction (Benson et al.,
662 2020). During hydration reactions, nominally incompatible elements may partition into mineral
663 phases due to the variable H_2O activity in fluids (Svenson et al., 1999, 2001). Svenson et al.
664 (2001) theorised that during hydration reactions Br/Cl ratios remain constant until the H_2O
665 content is reduced to a level whereby Cl may be removed from solution by crystallisation of

hydrous minerals (e.g., amphibole, apatite), as shown by the representative 'hydration trend' on **Figure 5c** from Svenson et al. (2001). As seen in the mineral separate from the pegmatoid (ST_16_009), amphibole is preferentially enriched in Cl over Br and consequently has a low Br/Cl ratio. The pegmatoid bodies in the Ultramafic and Banded Series are assumed to be representative of fluid-saturated residual fluids migrating through the partially-crystallized cumulate layers (Braun et al., 1994; Hanley et al., 2008). Hence, the enriched Br/Cl ratios in these pegmatoids (**Fig. 5c**) may be the result of preferential removal of Cl by the crystallisation of hydrous minerals occurred at a late-stage in the solidification of the intrusion at low fluid/rock ratios.

An interesting feature of the Stillwater data presented here is the remarkably consistent I/Cl and Br/Cl ratios observed across different parts of the intrusion (i.e., the Ultramafic Series and Banded Series), separated by ~1.5 km of stratigraphy. It is also worth noting that there are no apparent groupings in Br/Cl (and I/Cl) between samples that are hydrous mineral-bearing and those that are hydrous mineral-poor (**Fig. 5c**). As noted above, we take this commonality as suggesting the action of either one fluid phase throughout the entirety of the complex, or a shared fluid source (i.e., same provenance). Hanley et al. (2008) described populations of fluid inclusions from a pegmatite-hosted quartz in the LBS, as well as olivine-hosted inclusions from the BZ of the Ultramafic Series. The high temperature fluid inclusions were observed from both localities, and comprise halide melt and brine compositions, as well as carbonic fluids in the pegmatite quartz. Based upon microthermometric data, Hanley et al. (2008) proposed that the range of fluid inclusion compositions reflected a magmatic to hydrothermal continuum, to temperatures as low as ~480ºC. The hydrosaline and carbonic fluids are considered by the latter authors to have exsolved from different parts of the cumulate pile (rather than unmixed from one fluid); CO_2 should exsolve first because its solubility is lower than Cl (Webster et al., 1999; Webster, 2004). Hence, Hanley et al. proposed that the carbonic fluid exsolved from a hotter and shallower area of the cumulate pile with CO_2 saturated interstitial liquids, whilst the hydrosaline fluid was exsolved from a deeper part of the cumulate pile that had already lost

693 CO_2 during crystallisation. The two distinct fluids were subsequently trapped in the pegmatoids
694 that acted as pathways for both fluids, albeit without these fluids fully equilibrating with one
695 other. Density-dependent differential partitioning is thought to fractionate Br and Cl in
696 hydrothermal fluids; for example, Foustoukos and Seyfried (2007) found that Br would
697 preferentially partition into the low salinity vapour phase over brines. The presence of two (or
698 more) fluid or volatile phases in the Stillwater intrusion, as described above, indicates a
699 possible mechanism for the fractionation of heavy halogens; however, this does not seem to
700 be consistent with our observations of consistent halogen ratios for the Stillwater sample set.

701 A large range in salinities was also observed by Hanley et al. (2008) between different
702 pegmatoid bodies, which was taken as evidence of changing salinity during entrapment. This
703 variation was attributed by Hanley et al. (2008) to potentially result from a range of processes
704 such as (1) brine exsolution from different batches of residual liquid; (b) a single batch of
705 residual silicate liquid exsolving successive brines that became depleted in incompatible
706 elements; (c) variable mixing by interaction with wall rocks; or (d) incomplete mixing between
707 different brine batches before entrapment. Whilst the resolution of sampling undertaken in this
708 study is insufficient to fully discriminate between these possibilities, the similarity in halogen
709 ratios throughout the sample set points towards a process whereby all fluids have a common
710 provenance. Building on the observations of Hanley et al. (2008), the halogen-rich fluids that
711 subsequently operated throughout the Ultramafic and Banded Series may conceivably have
712 exsolved from a single batch of residual liquid, or residual liquids that were well-mixed.
713 Burgess et al. (2009) attributed high Br/Cl and I/Cl ratios in diamonds from the Panda
714 kimberlite (Canada) to halogen fractionation during the separation of silicic and immiscible
715 saline fluids. This process leads to enrichment of Br and I relative to Cl, as the heavier
716 halogens should be preferentially concentrated in the brine fraction (Bureau et al., 2000;
717 Broadley et al., 2018). The trend towards higher I/Cl and Br/Cl ratios, which is exhibited by the
718 pegmatoid samples (ST_16_003 and ST_16_009) in particular, may therefore be the result of
719 the separation of an immiscible brine phase, similar to that described by Hanley et al. (2008).

In summary, our new halogen data are permissive of halogen-rich fluids circulating throughout at least the Ultramafic and Lower Banded Series during solidification of the Stillwater intrusion. The Stillwater mantle source (and thus parental magma) was possibly somewhat enriched in Br/Cl relative to MORB but underwent variable degrees of crustal contamination following dehydration of the footwall country rocks. The exsolution of an immiscible hydrosaline fluid from solidifying cumulates led to (further) fractionation of Br/Cl and I/Cl, and the progressive Br/Cl enrichment observed in the pegmatoids (**Fig. 5c**) was potentially enhanced by the removal of Cl by crystallization of hydrous minerals resulting from hydrous melting and recrystallisation of the Stillwater cumulate pile. Our observations indicate that the halogen budgets of our samples can largely be explained by the observed mineral phases, although we cannot rule out an additional partial control by fluid inclusions, for example in the pegmatites. On the basis of the well-developed correlations observed in the halogen abundances of all samples, we suggest that the fluid phase preserved in inclusions in both the Ultramafic and Lower Banded Series of the Stillwater intrusion and described by Hanley et al. (2008) was the same one responsible for high temperature metasomatism (e.g., scapolisation) observed in the materials described here. Our halogen data do not bear substantially on the current controversy around the possible out-of-sequence emplacement of the Stillwater Complex (Wall et al., 2018). However, if both the Ultramafic and Lower Banded Series were affected by the same metasomatic event, this raises interesting questions for the timescales involved given that some rocks in the Ultramafic Series are purportedly >1 Myr older than the J-M Reef.

Implications for PGE mineralization

Investigations by Zientek et al. (2002) and Barnes et al. (2016) highlighted that the G Chromitite has lower concentrations of Pt + Pd (10 to 40 ppb) compared to many of the other chromitite layers; for example, concentrations of 300 to 3000 ppb Pt + Pd have been reported for the A and B chromitites. Barnes et al. (2016) also reported sulfur-loss from the chromitites for which they suggested several mechanisms; in the context of a hydromagmatic model they

suggested that the PGE are exsolved from sulfides during dissolution by a fluid. Palladium and Pt are preferentially removed from some layers, whereas the rest of the PGE are then sited in platinum group minerals included in the chromite. A weakness of this model is the lack of certainty surrounding the capability of a fluid in transporting Pd and Pt (Barnes et al., 2016). We also note that we observed no hydrous mineral phases in our samples of the G Chromitite (ST_16_002), which does not directly favour a hydromagmatic model. However, Spandler et al. (2005) has previously reported hydrous polyphase inclusions in G Chromitite Cr-spinel. Despite the apparent absence of hydrous minerals in our G Chromitite samples, ST_16_002 exhibits higher Cl and Br contents than the associated pegmatoid (ST_16_003), and the latter contains chlorapatite (**Fig. 4a, b**). It is clear that the magmas that formed the G Chromitite were either very enriched in Br/Cl or later interaction between cumulate and volatile-enriched fluids occurred. If it is the latter, the absence of hydrous minerals, S-loss and lower Pt + Pd ore tenor that generally characterise the G Chromitite might be explained by fluid migration away from this layer.

The J-M Reef samples (ST_16_004 and ST_16_008) reveal relatively high Cl and Br contents (26 – 320 ppm Cl, 223 – 2934 ppb Br) that are amongst the most enriched in our sample set. One of the key concepts of the 'volatile-refining' model is that sulfides and PGE are resorbed from cumulates and transported by Cl-enriched fluids to form a reef stratigraphically higher in the intrusion (e.g., Boudreau, 1999). Field observations of PGE-rich discordant pegmatoids support the late-stage mobilisation of the precious metals (e.g., Zientek et al., 2002). Other key evidence that supports a hydromagmatic origin for the J-M Reef is summarised in Boudreau (2016) and includes the presence of hydrous melt inclusions (now crystallised to polymineralic assemblages) in olivine and Cr-spinel.

As noted earlier, the PGE have been shown to be soluble at ppm-levels (at mildly oxidising conditions) in high (>500 °C) temperature brines (e.g., Pt-saturated brines with solubilities up to 16 ± 10 ppm [at 800 °C] are sufficiently PGE-enriched to form economically significant mineralisation; Simon and Pettke, 2009). Accepting the hydromagmatic model, which the

774 combined halogen data and mineralogical characteristics reported here do support, then the
775 enhanced halogen abundances in mineralised J-M Reef (ST_16_004) and associated
776 pegmatites lend weight to the idea of volatile-activity during PGE-enrichment. The sulfide-
777 deficient J-M Reef sample (ST_16_008) exhibits lower halogen contents than its sulfide-
778 bearing counterpart (ST_16_004), and no apatite (or Cl enrichment in hydrous minerals).
779 Boudreau (1995) highlighted a section between the Stillwater River and East Fork of the
780 Stillwater River, identified during mine development by the Stillwater Mining Company, where
781 the OB-I cuts downwards to form an 'unconformity' where sulfide mineralisation may be less
782 abundant or locally absent. This feature was ascribed by that study to slumping and localised
783 loss of reactive volatile-rich mush. Similarly, lateral changes in PGE and sulfide content in the
784 J-M Reef are often recorded in the Stillwater Mine and are often associated with ballrooms
785 (see Boudreau et al. 2021). These features are anomalously wide areas (minimum 6 metres
786 thickness and 5 metres width) within/below the J-M Reef, which are generally characterised
787 by sulfide contents of 1-2 vol% (compared to 0.5-1 vol% in 'normal' reef; Todd et al. 1982) but
788 may host increased levels of Pt and Pd (Harper, 2004; Childs et al., 2002). Harper (2004)
789 proposed several mechanisms to explain ballroom formation, including; local permeability
790 contrasts in the cumulate pile, higher fluid saturation resulting from greater melt interaction, or
791 variations in fluid volume across the complex. The overall lower halogen contents of sample
792 ST_16_008 compared to ST_16_004 may support a model of localised volatile loss such as
793 that described by Boudreau (1995, 2016) for the Stillwater River - East Fork locality, or at the
794 very least differences in volatile activity, to account for low sulfide mineralization in the Frog
795 Pond Adit section of the reef as observed in this study.

796 Experimental studies by Mungall and Brenan (2003) have shown that sulfide melt may be
797 capable of dissolving ppm levels of halogens and found that fluids or halide melts extracted
798 from the exsolved sulfide melts (isolated from silicate melts) would be characterised by high
799 Cl/Br (i.e., low Br/Cl) ratios (Lecumberri-Sanchez and Bodnar, 2018). The sulfide separates
800 from the J-M Reef sample (ST_16_004) reveal higher Br/Cl and I/Cl ratios (but lower halogen

contents) compared to their bulk rock counterparts. Our observations thus suggest that Br and I are preferentially enriched in the sulfides over Cl, in agreement with suggestions that Cl, Br and I display increasingly chalcophile behaviour with increasing atomic radii (i.e., $D_{Cl}^{sul\ liq\text{-}sil\ melt} < D_{Br}^{sul\ liq\text{-}sil\ melt} < D_{I}^{sul\ liq\text{-}sil\ melt}$; Steenstra et al., 2020). Recently published heavy halogen data from the Rum layered intrusion also appear to show I-enrichment of sulfide separates compared to bulk rocks, with higher Br/Cl and I/Cl ratios for sulfides compared to their respective whole rock values (Parker et al. 2019).

Our results are consistent with the suggestion of Mungall and Brenan (2003) that halogens may be stored and/or transported by sulfide liquids. Furthermore, Mungall and Brenan (2003) presented evidence of a link between magmatic sulfide liquids and halide minerals in the formation of the Pt, Pd, Au and Cu rich veins of the Fraser Copper Zone in the Sudbury Complex, which exhibits evidence of alteration haloes characterised by high Cl/Br ratios (low Br/Cl ratios; Jago et al. 1994). They proposed a mechanism whereby fluids or halide melts were expelled from a sulfide magma during the final stages of solidification. The suggestion that segregated fluid or halide melt exsolved from sulfide liquid would be characterised by a low Br/Cl ratio (Mungall and Brenan, 2003) also has interesting implications for the trends highlighted in this study; some of the lowest Br/Cl ratios of this sample set are observed in the J-M Reef (i.e., MORB-like; **Fig. 5**). Hence, the relationship between sulfide liquid and halogen-enriched fluids may be critically important in the formation of sulfide-hosted precious metal ore deposits and the recognition of extreme halogen fractionation resulting from sulfide-liquid and halogen interaction requires further investigation in this context.

Implications

Heavy halogen data of samples from the Stillwater Complex highlight extreme enrichment of Br/Cl linked to the activity of fluids during late-stage metasomatic processes operating in the intrusion. Alteration phases in some samples (e.g., scapolite and amphiboles in ST_16_009) also lend support to the activity of high temperature metasomatic fluids at the postcumulus stage. In the J-M Reef, low I/Cl ratios point towards a magmatic origin for the fluids rather than

828 significant halogen addition from an external source. In contrast, mildly-enriched I/Cl ratios
829 and contents for the pegmatoids and the G Chromitite may preserve evidence of minor crustal
830 contamination. The exsolution of a volatile-rich fluid led to the fractionation of the halogens,
831 and progressive depletion of Cl relative to Br by preferential incorporation of the former in
832 hydrous minerals further enriched Br/Cl in fluid-saturated residual fluids, as represented by
833 the pegmatoid bodies. This Br/Cl rich fluid may then have interacted with newly-injected hotter
834 magmas, causing reprecipitation of sulfides and PGE and the formation of the J-M Reef.
835 Enriched Br/Cl and I/Cl ratios for the sulfide separates of the J-M Reef highlight the relatively
836 chalcophilic behaviour of Br and I compared to Cl; these fractionations have been observed
837 in other magmatic sulfide-hosted ore deposits and suggest that halogen behaviour during
838 sulfide liquid differentiation/crystallisation is an important avenue of future investigation.

839

840 **Acknowledgements:** This manuscript forms a component of A. Parker's PhD thesis
841 undertaken at the University of Manchester, supported by the Natural Environment Research
842 Council grant number NE/L002469/1. The samples studied here were collected during the
843 2016 Penrose Conference on the Stillwater Complex, and the authors are grateful to all
844 participants of that meeting for stimulating petrological discussions and debates. Jon Fellowes
845 and Lewis Hughes are thanked for their technical support with the EPMA and SEM analyses.
846 John Cowpe and Lydia Fawcett are thanked for assistance with sample irradiation and
847 Lorraine Ruzié-Hamilton for her assistance with NI-NGMS analyses. Sarah-Jane Barnes and
848 an anonymous reviewer are thanked for their detailed review comments, as is Justin Filiberto
849 for his editorial handling of our manuscript.

References Cited

Abbott, Jr., D.M., Bullock, R.L., Gibbs, B., and Kunter, R.S. (2011). Technical report for the mining operations at Stillwater Mining Company, Stillwater Mine, 45°23′N, 109°53′W, East Boulder Mine, 45°30′N, 109°05′W: Denver, Colorado, Behre Dolbear & Company Ltd., Project 11-030, 87 pp. URL: http://secfilings.nyse.com/filing.php?ipage=7682024.

Aiuppa, A., Baker, D.R., and Webster, J.D. (2009). Halogens in volcanic systems. Chemical Geology, 263, 1-18.

Barnes, S. J., Page, P., Prichard, H.M., Zientek, M.L., and Fisher, P.C. (2016). Chalcophile and platinum-group element distribution in the Ultramafic series of the Stillwater Complex, MT, USA - implications for processes enriching chromite layers in Os, Ir, Ru, and Rh. Mineralium Deposita, 51, 1–23.

Bazarkina, E.F., Pokrovski, G.S. and Hazemann, J-L. (2014). Structure, stability and geochemical role of palladium chloride complexes in hydrothermal fluids. Geochimica et Cosmochimica Acta 146, 107-131.

Benson, E., Connolly, J.A.D., and Boudreau, A.E. (2020). Crustal fluid contamination in the Bushveld Complex, South Africa: An analogue for subduction zone fluid migration. International Geology Review. doi.org/10.1080/00206814.2020.1795734.

Berndt M.E., and Seyfried W.E. (1997) Calibration of Br/Cl fractionation during subcritical phase separation of seawater: possible halite at 9 to 10 N East Pacific Rise. Geochimica Cosmochimica Acta 61, 2849–2854.

Boneß M., Heumann K.G., and Haack. U. (1991) Cl, Br and I analyses of metamorphic and sedimentary rocks by isotope dilution mass spectrometry. Contributions to Mineralalogy and Petrology, 107(1), 94–99.

874 Boudreau, A.E. (1988). Investigations of the Stillwater Complex, IV. The role of volatiles in the
875 petrogenesis of the J-M reef, Minneapolis adit section. Canadian Mineralogist 26, 193–208.

876 Boudreau, A.E. (1995). Crystal aging and the formation of fine-scale layering. Mineralogy and
877 Petrology, 54, 55–69.

878 Boudreau, A.E. (1999). Fluid Fluxing of Cumulates: the J-M Reef and Associated Rocks of the
879 Stillwater Complex, Montana. Journal of Petrology, 40(5), 755–772.

880 Boudreau, A.E. (2016). The Stillwater Complex, Montana—overview and the significance of
881 volatiles. Mineralogical Magazine 80, 585–637.

882 Boudreau, A.E., Mathez, E.A., and McCallum, I.S. (1986). Halogen geochemistry of the
883 Stillwater and Bushveld Complexes: evidence for transport of the platinum-group elements by
884 Cl-rich fluids. Journal of Petrology, 27, 967-986.

885 Boudreau, A.E., and McCallum, I.S. (1986). Investigations of the Stillwater Complex. Part III.
886 The Picket Pin Pt/ Pd deposit. Economic Geology, 81, 1953-1975.

887 Boudreau, A.E., and McCallum, I.S. (1989). Investigations of the Stillwater Complex: Part V.
888 Apatite as indicators of evolving fluid composition. Contributions to Mineralogy and Petrology,
889 102, 138–153.

890 Boudreau, A.E., and McCallum, I.S. (1990). Low temperature alteration of REE-rich
891 chlorapatite from the Stillwater Complex, Montana. American Mineralogist 75, 687-693.

892 Boudreau, A.E., and McCallum, I.S. (1992). Concentration of platinum- group elements by
893 magmatic fluids in layered intrusions. Economic Geology 87, 1830-1848.

894 Boudreau, A.E., and Meurer, W.P. (1999). Chromatographic separation of the platinum-group
895 elements, base metals, gold and sulfur during degassing of a compacting and solidifying
896 igneous crystal pile. Contributions to Mineralogy and Petrology, 134, 174-185.

897 Boudreau, A.E., Stewart, M.A., and Spivack, A.J. (1997). Stable Cl isotopes and origin of high-
898 Cl magmas of the Stillwater Complex, Montana. Geology, 25(9), 791–794.

899 Boudreau, A.E., Butak, K.C., Geraghty, E.P., Holick, P.A. and Koski, M.S. (2021). Mineral
900 deposits of the Stillwater Complex. Montana Bureau of Mines and Geology Special Publication
901 122, Geology of Montana 2, Special Topics, 33 pp.

902 Braitsch O. (1971) Salt Deposits; Their Origin and Composition. Springer-Verlag.

903 Brazzle, R.H., Pravdivtseva, O.V., Meshik, A.P and Hohenberg, C.M. (1999) Verification and
904 interpretation of the I-Xe chronometer. Geochimica et Cosmochimica Acta. 63, 739-760.

905 Broadley, M.W., Kagi, H., Burgess, R., Zedgenizov, D. Mikhail, S. Almayrac, M., Ragozin, A.,
906 Pomazansky, B., and Sumino, H. (2018). Plume-lithosphere interaction, and the formation of
907 fibrous diamonds. Geochemical Perspectives Letters, 8, 26-30.

908 Bureau, H., Keppler, H., and Métrich, N. (2000). Volcanic degassing of bromine and iodine:
909 experimental fluid/melt partitioning data and applications to stratospheric chemistry. Earth and
910 Planetary Science Letters, 183, 51-60.

911 Burgess, R., Cartigny, P., Harrison, D., Hobson, E., and Harris, J. (2009). Volatile composition
912 of microinclusions in diamonds from the Panda kimberlite, Canada: Implications for chemical
913 and isotopic heterogeneity in the mantle. Geochimica et Cosmochimica Acta 73, 1779-1794.

914 Campbell I.H., and Barnes S.J. (1984) A model for the geochemistry of the platinum-group
915 elements in magmatic sulfide deposits. Canadian Mineralogist, 22, 151-160.

916 Chavrit, D., Burgess, R., Sumino, H., Teagle, D.A., Droop, G., Shimizu, A., and Ballentine,
917 C.J. (2016). The contribution of hydrothermally altered ocean crust to the mantle halogen and
918 noble gas cycles. Geochimica et Cosmochimica Acta, 183, 106-124.

919 Childs, J.F., Evans, J.R., Wood, K.Y., Koski, M.S. and Evans, J.D. (2002). Some preliminary
920 descriptive aspects of ballroom mineralization at the Stillwater palladium-platinum Mine,

921 Stillwater Mining Company, Nye, Montana. Pp. 91–92 in: 9th International Platinum
922 Symposium, Abstract with Program, 21–25 July 2002. Billings, Montana, USA.

923 Czamanske, G.K., and Loferski, P.J. (1996). Cryptic trace-element alteration of anorthosite,
924 Stillwater Complex, Montana. Canadian Mineralogist, 34, 559-576.

925 DePaolo, D.J. and Wasserburg, G.J. (1979). Sm-Nd age of the Stillwater Complex and the
926 mantle evolution curve for neodymium. Geochimica et Cosmochimica Acta, 43, 999–1008.

927 Engvik, A. K., Mezger, K., Wortelkamp, S., Bast, R., Corfu, F., Korneliussen, A., Ihlen, P.,
928 Bingen, B., and Austrheim, H. (2011). Metasomatism of gabbro – mineral replacement and
929 element mobilization during the Sveconorwegian metamorphic event. Journal of Metamorphic
930 Geology, 29, 399-423.

931 Engvik, A. K., Taubald, H., Solli, A., Grenne, T., and Austrheim, H. (2018). Dynamic
932 Metasomatism: Stable Isotopes, Fluid Evolution, and Deformation of Albitite and Scapolite
933 Metagabbro (Bamble Lithotectonic Domain, South Norway). Geofluids, 2018, 1-22.

934 Finn, C.A., Zientek, M.L., Bloss, B. R., Wintzer, N.E. and Parks, H.L. (2013). Geophysical
935 imaging of the Stillwater Complex and relation to platinum group element exploration.
936 Geological Society of America, 2013 Annual Meeting, Paper No. 109–6.

937 Finn, C.A., Zientek, M.L., Bloss, B.R., Bedrosian, P., Cole, J., Webb, S.J. and Parks, H.L.
938 (2016). Geophysical imaging of the extents of the Stillwater Complex and northern lobe of the
939 Bushveld Complex and relation to platinum group element exploration. In: Layered Mafic
940 Intrusions and Associated Economic Deposits, Geological Society of America Penrose
941 Conference, Red Lodge, Montana, p. 26.

942 Foustoukos, D.I., and Seyfried, W.E. (2007). Trace element partitioning between vapor, brine
943 and halite under extreme phase separation conditions. Geochimica et Cosmochimica Acta,
944 71, 2056–2071.

945 Gammons, C.H. (1996). Experimental investigations of the hydrothermal geochemistry of
946 platinum and palladium: V. Equilibria between platinum metal, (Pt(II), and Pt(IV) chloride
947 complexes at 25 to 300 °C. Geochimica et Cosmochimica Acta 60(10), 1683-94.

948 Godel, B., and Barnes, S.J. (2008). Platinum-group elements in sulfide minerals and the whole
949 rocks of the J-M Reef (Stillwater Complex): Implication for the formation of the reef. Chemical
950 Geology, 248(3-4), 272–294.

951 Hanley, J.J., and Koga, K.J. (2018). Halogens in Terrestrial and Cosmic Geochemical
952 Systems: Abundances, Geochemical Behaviors, and Analytical Methods. In: Harlov, D.E.,
953 Aranovich, L. (Eds.), The Role of Halogens in Terrestrial and Extraterrestrial Geo-chemical
954 Processes. Springer International Publishing, Switzerland.

955 Hanley, J.J., Mungall, J.E., Pettke, T., Spooner, E.T.C., and Bray, C.J. (2008). Fluid and halide
956 melt Inclusions of magmatic origin in the ultramafic and lower banded series, Stillwater
957 complex, Montana, USA. Journal of Petrology, 49(6), 1133-1160.

958 Hanley, J.J., Pettke, T., Mungall, J.E., and Spooner, E.T.C. (2005). The solubility of platinum
959 and gold in NaCl brines at 1.5 kbar, 600 to 800°C: A laser ablation ICP-MS pilot study of
960 synthetic fluid inclusions. Geochimica et Cosmochimica Acta, 69(10), pp.2593–2611.

961 Harper, M.P. (2004) Platinum Group Element Mineralization in "Ballrooms" of the J-M Reef of
962 the Stillwater Complex, Montana. Unpublished MS thesis, Brigham Young University, Provo,
963 USA.

964 Holland, G., and Ballentine, C.J. (2006). Seawater subduction controls the heavy noble gas
965 composition of the mantle. Nature, 441, 186–191.

966 Horan, M.F., Morgan, J.W., Walker, R.J. and Cooper, R.W. (2001). Re-Os isotopic constraints
967 on magma mixing in the Peridotite zone of the Stillwater Complex, Montana, USA.
968 Contributions to Mineralogy and Petrology 141, 446–457.

969 Jago, B.C., Morrison, G.G., and Little, T.L. (1994). Metal zonation patterns and microtextural
970 and micromineralogical evidence for alkali- and halogen-rich fluids in the genesis of the Victor
971 Deep and McCreedy East footwall copper orebodies, Sudbury Igneous Complex. In
972 Proceedings of the Sudbury – Noril'sk Symposium (P.C. Lightfoot & A.J. Naldrett, eds.).
973 Ontario Geological Survey, Special Volume 5, 65-75.

974 Jones, W.R., Peoples, S.W. and Howland, A.L. (1960). Igneous and tectonic structures of the
975 Stillwater Complex, Montana. U.S. Geological Survey Bulletin, 1071, 281–340.

976 Kendrick, M.A. (2012) High precision Cl, Br and I determnations in mineral standards using
977 the noble gas method. Chemical Geology, 292-293, 116-126.

978 Kendrick, M.A., Arculus, R.J., Burnard, P., and Honda, M. (2013). Quantifying brine
979 assimilation by submarine magmas: examples from the Galápagos Spreading Centre and Lau
980 Basin. Geochimica Cosmochimica Acta,123, 150–165.

981 Kendrick, M.A., Hémond, C., Kamenetsky, V.S., Danyushevsky, L., Devey, C.W., Rodemann,
982 T., Jackson, M.G., and Perfit, M.R. (2017). Seawater cycled throughout Earth's mantle in
983 partially serpentinized lithosphere. Nature Geoscience, 10(3), 222-228. DOI:
984 10.1038/ngeo2902

985 Kendrick, M.A., Jackson, M.G., Kent, A. J.R., Hauri, E.H., Wallace, P.J., and Woodhead, J.
986 (2014). Contrasting behaviours of CO_2, S, H_2O and halogens (F, Cl, Br, and I) in enriched-
987 mantle melts from Pitcairn and Society seamounts. Chemical Geology, 370, 69-81. DOI:
988 10.1016/j.chemgeo.2014.01.019

989 Kendrick, M.A., Kamenetsky, V., Phillips, D., and Honda, M. (2012a) Halogen systematics (Cl,
990 Br, I) in Mid-Ocean Ridge Basalts: a Macquarie Island case study. Geochimica et
991 Cosmochimica Acta, 81, 82–93.

992 Kendrick, M.A., Woodhead, J.D., and Kamenetsky, V.S (2012b). Tracking halogens through
993 the subduction cycle. Geology, 40, 1075–1078.

994 Korzhinskiy, M. A. (1982). Apatite solid solutions as indicators of the fugacity of HCl^o and HF^o
995 in hydrothermal fluids. Geochemistry Int. 1981, 44-60.

996 Kusebauch, C., John, T., Whitehouse, M. J., Klemme, S., and Putnis, A. (2015). Distribution
997 of halogens between fluid and apatite during fluid-mediated replacement processes.
998 Geochimica et Cosmochimica Acta, 170, 225-246.

999 Labotka, T.C., and Kath, R.L. (2001). Petrogenesis of the contact- metamorphic rocks beneath
1000 the Stillwater Complex, Montana. Geological Society of America Bulletin, 113, 1312-1232.

1001 Latypov, R. M. (2019). Comment on “The Stillwater Complex: integrating zircon
1002 geochronological and geochemical constraints on the age, emplacement history and
1003 crystallization of a large, open-system layered intrusion” by Wall et al. (J. Petrology, 59, 153–
1004 190, 2018). J. Petrol. 59, 153–190.

1005
1006 Lechler, P.J., Arehart, G.B., and Knight, M. (2002). Multielement and isotopic geochemistry of
1007 the J-M Reef, Stillwater Intrusion, Montana. In: Boudreau, A (ed.) Proceedings of the Ninth
1008 International Platinum Symposium, 245-248.

1009 Lecumberri-Sanchez P., and Bodnar, R.J. (2018). Halogen Geochemistry of Ore Deposits:
1010 Contributions Towards Understanding Sources and Processes. In: Harlov, D.E. and Aranovich
1011 L., (Eds.) The Role of Halogens in Terrestrial and Extraterrestrial Geochemical Processes.
1012 Springer International Publishing, Switzerland.

1013 Li, Y-H and Schoonmaker, J.E. (2003) Chemical Composition and Mineralogy of Marine
1014 Sediments. Treatise on Geochemistry, Executive Editors: Heinrich D. Holland and Karl K.
1015 Turekian. pp. 407. Elsevier, 1-35.

1016 Liebscher A., Luders V., Heinrich W., and Schettler G. (2006) Br/Cl signature of hydrothermal
1017 fluids: liquid-vapour fractionation of bromine revisited. Geofluids 6, 113–121.

1018 Matsuda, J., and Nagao, K. (1986). Noble-gas abundances in a deep-sea sediment core from
1019 eastern equatorial Pacific. Geochemical Journal, 20, 71–80.

McBirney, A. R. (2002). The Skaergaard layered series: Part VI, excluded trace elements. Journal of Petrology 43, 535-556.

McCallum, I.S. (1996). The Stillwater Complex. Developments in Petrology, 15(C), 441–483.

McCallum, M.E., Loucks, R.R., Carlson, R.R, Cooley, E.F., and Doerge, T. A. (1976). Platinum metals associated with hydrothermal copper ores of the New Rambler mine, Medicine Bow Mountains, Wyoming. Economic Geology. 71, 1429-51.

McCallum, I.S., Thurber, M.W., O'Brien, H.E. and Nelson, B.K. (1999). Lead isotopes in sulfides from the Stillwater Complex, Montana: evidence for subsolidus remobilization. Contributions to Mineralogy and Petrology 137, 206-219.

McCallum, I.S., Raedeke, L.D. and Mathez, E.A. (1980). Investigations of the Stillwater Complex, I. Stratigraphy and structure of the Banded zone. American Journal of Science, 280A, 59-87.

Meurer, W.P., Klaber, S.A. and Boudreau, A.E., (1997). Discordant bodies from Olivine-Bearing zones III and IV of the Stillwater Complex, Montana -Evidence for post-cumulus fluid migration in layered intrusions. Contributions to Mineralogy and Petrology, 130, 81-92.

Meurer,W. P., Willmore, C. C. and Boudreau, A. E. (1999). Metal redistribution during fluid exsolution and migration in the Middle Banded series of the Stillwater Complex, Montana. Lithos, 47, 143-156.

Mogk, D.W. and Mueller, P.A. (1990) Evidence for Archean accretionary tectonics in the northern Wyoming Province, SW Montana. Geological Society of America Abstracts with Programs, 22, 262.

Moreira, M., Kunz, J., and Allègre, C., (1998). Rare gas systematics in popping rock: isotopic and elemental compositions in the upper mantle. Science, 279, 1178–1181.

Mungall, J.E., and Brenan, J.M., (2003). Experimental evidence for the Chalcophile behavior of the halogens. Canadian Mineralogist, 41(1), 207–220.

1045 Muramatsu, Y. and Wedepohl, K.H., (1998). The distribution of iodine in the Earth's crust.
1046 Chemical Geology, 147, 201-216.

1047 Nunes, P.D. and Tilton, G.R. (1971) Uranium-lead ages of minerals from the Stillwater
1048 Complex and associated rocks, Montana. Geological Society of America Bulletin, 82, 2231–
1049 2250.

1050 O'Driscoll, B, and VanTongeren, J.A., (2017). Layered Intrusions: From Petrological
1051 Paradigms to Precious Metal Repositories. Elements, 13(6), 383–389.

1052 Oosting S. E. and Von Damm K. L. (1996) Bromide/chloride fractionation in seafloor
1053 hydrothermal fluids from 9–10^{o}N east Pacific rise. Earth and Planetary Science Letters, 144,
1054 133–145.

1055 Page, N. J. (1976). Serpentinization and alteration in an olivine cumulate from the Stillwater
1056 Complex, southwestern Montana. Contributions to Mineralogy and Petrology, 54, 127-137.

1057 Page, N. J. (1977). Stillwater Complex, Montana: rock succession, metamorphism, and
1058 structure of the complex and adjacent rocks. US Geological Survey Professional Paper, 999.

1059 Page, N.J., (1979). Stillwater Complex, Montana: Structure, mineralogy, and petrology of the
1060 Basal Zone with emphasis on the occurrence of sulphides. U.S Geological Survey
1061 Professional Paper 1038, 69 pp.

1062 Page, N. J. and Zientek, M. L. (1985) Petrogenesis of metamorphic rocks beneath the
1063 Stillwater Complex: Lithologies and structures. In Stillwater Complex, Montana: Geology and
1064 Guide (eds. G. K. Czamanske and M. L. Zientek). Montana Bureau of Mines and Geology,
1065 Special Publication 92, Billings, Montana. 55–69.

1066 Page, N.J. and Zientek, M.L. (1987). Composition of primary postcumulus amphibole and
1067 phlogopite within an olivine cumulate in the Stillwater Complex, Montana. US Geological
1068 Survey Bulletin, 1674-A.

1069 Page, N.J, Zientek, M.L., Czamanske, G.K. and Foose, M. P. (1985). Sulfide mineralization in
1070 the Stillwater Complex and underlying rocks. Pp. 93–96 in: Stillwater Complex, Montana:
1071 Geology and Guide (G.K. Czamanske and M.L. Zientek, editors), Montana Bureau of Mines
1072 and Geology Special Publication, 92. Billings, Montana, USA.

1073 Parker, A. P., Clay, P. L., Burgess, R., Balcone-Boissard, H., Bürckel, P., and O'Driscoll, B.,
1074 (2019). Halogen cycling and precious metal enrichment in sub-volcanic magmatic systems:
1075 insights from the Rum layered intrusion, Scotland. Earth and Planetary Science Letters,
1076 115769.

1077 Parsons I (ed) (1987). Origins of Igneous Layering. D. Reidel, Dordrecht, 663 pp
1078
1079 Piccoli, P., and Candela, P., 1994, Apatite in felsic rocks: A model for the estimation of initial
1080 halogen concentrations in the Bishop Tuff (Long Valley) and Tuolumne intrusive suite (Sierra
1081 Nevada batholith) magmas: American Journal of Science, 294, 92–135

1082 Premo, W., Helz, R., Zientek, M. and Langston, R., (1990). U-Pb and Sm-Nd ages for the
1083 Stillwater Complex and its associated sills and dikes, Beartooth Mountains, Montana:
1084 Identification of a parent magma?. Geology, 18, 1065-1068.

1085 Prichard, H.M., Barnes, S-J., Fisher, P.C., Page, P. and Zientek, M.L. (2017). Laurite and
1086 associated PGM in the Stillwater chromitites: implications for processes of formation, and
1087 comparisons with laurite in the Bushveld and ophiolitic chromitites. Canadian Mineralogist
1088 55(1), 121-144.

1089 Raedeke L.D., and McCallum, I. S., (1984). Investigations in the Stillwater Complex. Part II.
1090 Petrology and petrogenesis of the Ultramafic Series. Journal of Petrology, 25, 395-420.

1091 Ripley, E.M., Wernette, B.W., Ayre, A., Li, C., Smith, J.M., Underwood B.S., and Keays, R.R.,
1092 (2017). Multiple S isotope studies of the Stillwater Complex and country rocks: An assessment
1093 of the role of crustal S in the origin of PGE enrichment found in the J-M Reef and related rocks.
1094 Geochimica et Cosmochimica Acta, 214, 226–245.

1095 Ruzié-Hamilton, L., Clay, P. L., Burgess, R., Joachim, B., Ballentine, C. J., and Turner, G.,
1096 (2016). Determination of halogen abundances in terrestrial and extraterrestrial samples by the
1097 analysis of noble gases produced by neutron irradiation, Chemical Geology, 437, 77-87.

1098 Schannor, M., Veksler, I.V., Hecht, L., Harris, C., Romer, R.L. and Manyeruke, T.D. (2018).
1099 Small-scale Sr and O isotope variations through the UG2 in the eastern Bushveld Complex:
1100 The role of crustal fluids. Chemical Geology 485, 100-112.

1101 Schiffries, C. M. (1982). The platiferous dunite pipe in the Bushveld complex: infiltration
1102 metasomatism by a chloride solution. Economic Geology, 77, 1439-1453.

1103 Schilling, J. G., Bergeron, M. B., Evans, R., and Smith, J. V., (1980). Halogens in the Mantle
1104 Beneath the North Atlantic [and Discussion]. Philosophical Transactions of the Royal Society
1105 of London. Series A, Mathematical and Physical Sciences, 297, 147-178.

1106 Scholten, L., Watenphul, A., Beermann, O., Testemale, D., Ames, D. and Schmidt, C. (2018).
1107 Nickel and platinum in high-temperature H_2O + HCL fluids: Implications for hydrothermal
1108 mobilization. Geochimica et Cosmochimica Acta 224(1), 187-199.

1109 Scoates J.S., and Wall C.J., (2015). Geochronology of layered intrusions. In: Charlier B.,
1110 Namur O., Latypov R., Tegner C. (eds) Layered Intrusions. Dordrecht: Springer, 3–74.

1111 Simakin, A., Salova, T., Borisova, A.Y., Pokrovski, G.S., Shaposhnikova, O., Tyutyunnik, O.,
1112 Bondarenko, G., Nekrasov, A., and Isaenko, S.I. (2021). Experimental study of Pt solubility in
1113 the CO-CO_2 fluid and low f_{O2} and subsolidus conditions of the ultramafic-mafic intrusions.
1114 Minerals 11, 225.

1115 Smith J., Ripley E. M., and Li C., (2017) Variable genetic models for the origin of country rock-
1116 hosted massive sulfides. In Proceedings of the 14th Biennial SGA Meeting, Society of Geology
1117 Applied to Mineral Deposits Annual Meeting, Quebec City.

Spandler, C., Mavrogenes, J., and Arculus, R., (2005). Origin of chromitites in layered intrusions: Evidence from chromite-hosted melt inclusions from the Stillwater Complex. Geology, 33(11), 893-896.

Staudacher, T., and Allègre, C.J., (1988). Recycling of oceanic crust and sediments: the noble gas subduction barrier. Earth and Planetary Science Letters, 89, 173–183. DOI: 10.1016/0012-821X(88)90170-7

Steenstra, E.S., van Haaster, F., van Mulligen, R., Flemetakis, S., Berndt, J., Klemme, S., and van Westrenen, W., (2020). An experimental assessment of the chalcophile behavior of F, Cl, Br and I: Implications for the fate of halogens during planetary accretion and the formation of magmatic ore deposits. Geochimica et Cosmochimica Acta, 273, 275-290.

Stormer, J. C, and Carmichael, I. S. E., (1971). Fluorine-hydroxyl exchange in apatite and biotite: A potential igneous geothermometer. Contributions to Mineralogy and Petrology 31, 121-31.

Stumpfl, E. F. (1974). The genesis of platinum deposits: further thoughts. Minerals Science Engineering, 6, 120-141.

Stumpfl, E. F. and Rucklidge, J. C., (1982). The platiniferous dunite pipes of the eastern Bushveld Complex. Economic Geology, 77, 1419-1431.

Su, C., Bai, Y., Cui, M.M., Wang, J., Xiao, Y., Lenaz, D., Sakyi, P.A., Robinson, P.T., (2020). Petrogenesis of the Ultramafic Zone of the Stillwater Complex in North America: Constraints from mineral chemistry and stable isotopes of Li and O. Contributions to Mineralogy and Petrology 175, 68.

Sullivan, N.A., Zajacz, Z., Brenan, J.M., Hinde, J.C., Tsay, A. and Yin, Y. (2021). The solubility of gold and palladium in magmatic brines: Implications for PGE enrichment in mafic-ultramafic and porphyry environments. Geochimica et Cosmochimica Acta, in revision.

1143 Svensen, H., Banks, D.A., and Austreim, H., (2001). Halogen contents of eclogite facies fluid
1144 inclusions and minerals: Caledonides, western Norway. Journal of Metamorphic Geology 19,
1145 165–178.

1146 Tagirov, B.R., Filimonova, O.N., Trigub, A.L., Akinfiev, N.N., Nickolsky, M.S., Kvashnina, K.O.,
1147 Chareev, D.A. and Zotov, A.V. (2019). Platinum transport in chloride-bearing fluids and melts:
1148 Insights from in situ X-ray absorption spectroscopy and thermodynamic modelling.
1149 Geochimica et Cosmochimica Acta 254, 86-101.

1150 Thomson, J.A., (2008). Beneath the Stillwater Complex: Petrology and geochemistry of
1151 quartz-plagioclase-cordierite (or garnet)-orthopyroxene-biotite spinel hornfels, Mountain View
1152 area, Montana. American Mineralogist, 93(2-3), pp.438–450.

1153 Todd, S.G., Keith, D.W., LeRoy, L.W., Shissel, D.J., Mann, E.L. and Irvine, T.N., (1982). The
1154 J-M platinum palladium reef of the Stillwater Complex, Montana: I. Stratigraphy and petrology.
1155 Economic Geology, 77, 1454–1480.

1156 Turner, G., Huneke, J.C., Podosek, F.A., and Wasserburg, G.J., (1971). ^{40}Ar-^{39}Ar ages and
1157 cosmic ray exposure ages of Apollo 14 samples. Earth and Planetary Science Letters, 12, 19-
1158 35.

1159 Ulrich, T., Gunther, D. & Heinrich, C. A. (2001). The evolution of a porphyry Cu-Au deposit,
1160 based on LA-ICP-MS analysis of fluid inclusions; Bajo de la Alumbrera, Argentina. Economic
1161 Geology, 96, 1743-1774.

1162 Volborth, A. A.,Tarkian, M., Stumpfl, E. F. & Housley, R. M. (1986). A survey of the Pd-Pt
1163 mineralization along the 35 km strike of the J-M reef, Stillwater Complex, Montana. Canadian
1164 Mineralogist 24, 459-481.

1165 Volfinger, M., Roberts, J.-L., Vielzeuf, D. and Neiva, A.M.R., 1985. Structural control of the
1166 chlorine content of OH-bearing silicates (micas and amphiboles). Geochimica et
1167 Cosmochimica Acta 49, 37-48.

Von Damm K. L., Lilley M. D., Shanks W. C., Brockington M., Bray A. M., O'Grady K. M., Olson E., Graham A., Proskurowski G. and Sou E. P. R. S. P. (2003) Extraordinary phase separation and segregation in vent fluids from the southern East Pacific Rise. Earth Planet. Sci. Lett. 206, 365–378.

Wager LR, Brown GM (1968). Layered igneous rocks. Oliver and Boyd, London, 588 pp.

Wall, C. J., Scoates, J. S., Weis, D., Friedman, R. M., Amini, M., and Meurer, W., (2018). The Stillwater Complex: Integrating Zircon Geochronological and Geochemical Constraints on the Age, Emplacement History and Crystallization of a Large, Open-System Layered Intrusion. Journal of Petrology, 59(1), 153–190.

Webster, J. D. (2004). The exsolution of magmatic hydrosaline chloride liquids. Chemical Geology, 210, 33-48.

Webster, J. D., Kinzler, R. J. & Mathez, E. A. (1999). Chloride and water solubility in basalt and andesite melts and implications for magmatic degassing. Geochimica et Cosmochimica Acta, 63, 729-738.

Willmore, C. C., Boudreau, A. E. and Kruger, F. J. (2000). The halogen geochemistry of the Bushveld Complex, Republic of South Africa: Implications for chalcophile element distribution in the Lower and Critical zones. Journal of Petrology, 41, 1517-1539.

Willmore, CC., Boudreau, A. E., Spivack, A., and Kruger, F.J. (2002). Halogens of the Bushveld Complex, South Africa: □37Cl and Cl/F evidence for hydration melting of the source region in a back-arc setting. Chemical Geology, 182, 503-511.

Wooden, J. L., Czamanske, G. K. and Zientek, M. L. (1991). A lead isotopic study of the Stillwater Complex, Montana: constraints on crustal contamination and source regions. Contributions to Mineralogy and Petrology 107, 376–391.

Zientek, M. L., Cooper, R. W., Corson, S. R. and Geraghty, E. P. (2002). Platinum-group element mineralization in the Stillwater Complex. In: Cabri, L. (ed.) The Geology,

1194 Geochemistry, Mineralogy and Mineral Beneficiation of Platinum-Group Elements. Canadian
1195 Institute of Mining, Metallurgy and Petroleum, Special Volume 54, 459-481.

1196

1197

1198

1199

1200

1201

1202

1203

1204

1205

1206

1207

1208

1209

1210

1211

1212

1213

1214

Figure Captions

Figure 1. Geology of the Stillwater Complex, with the key PGE horizons the J-M Reef and Picket Pin highlighted. Inset in the top right displays the relationship of the Stillwater Complex to the surrounding Archean blocks and other country rocks (after Abbot et al., 2011). Ages for the Quartz monzonite and Stillwater Complex are from Wall et al. (2018) and hornfels age from Nunes and Tilton, (1971).

Figure 2. Schematic column through the Stillwater Complex, illustrating major stratigraphic units, mineral modes and apatite chemistry as a function of stratigraphic height. Modal olivine in poikilitic and granular harzburgite in the Ultramafic Series is based on average modes. The labels A through K in the Peridotite Zone signify the positions of the major chromitite bodies. The labels P and S illustrate positions in stratigraphy where pegmatoid bodies and sulfides are common. The locations of the J M reef and the Picket Pin PGE zone are also labelled. Modified after McCallum (1996) and Boudreau (2016).

Figure 3. (a) Photomicrograph (in cross-polarised light) of the G chromitite (ST_16_002), displaying chain textured chromitite surrounding olivine. (b) Photomicrograph (in cross-polarised light) of apatite in the pegmatoid below the G chromitite (ST_16_003). The orthopyroxene that encloses the apatite commonly contains exsolution of clinopyroxene. (c) Photomicrograph (in cross-polarised light) of the partially serpentinised J-M Reef (ST_16_004). (d) Photomicrograph (in cross-polarised light) of the S-poor J-M Reef (ST_16_008). (e) Photomicrograph (in cross-polarised light) of alteration phases in the pegmatoid vein below the J-M Reef (ST_16_011). Serpentine and talc appear to be pseudomorphing the original igneous mineralogy (possibly orthopyroxene and clinopyroxene). (f) Photomicrograph (in cross-polarised light) of the pegmatoid below the J-M Reef (ST_16_009). Scapolite has almost entirely replaced the pre-existing mineral, likely plagioclase. Not the many fluid inclusions in the quartz. (g) Photomicrograph (in cross-polarised light) of a relatively unaltered plagioclase feldspar with a corona of serpentine in ST_16_009. Serpentine and other alteration phases have otherwise entirely replaced the

igneous mineralogy. (h) Photomicrograph (in reflected light) of the massive sulfides below the Stillwater Complex contact (ST_16_005). Ap = apatite, Bt = biotite, Ol = olivine, Plg = plagioclase, Cpx = clinopyroxene, Opx = orthopyroxene, Scap = scapolite, Serp = serpentine, Qtz = quartz, Cr = chromite, Slf = sulfides, Chalc = chalcopyrite, Pyrr = pyrrhotite.

Figure 4. (a) Quantitative element map of Ca in the pegmatoid below the G chromitite (ST_16_003). (b) Quantified element map of Cl in the pegmatoid below the G chromitite (ST_16_003). Note the near end-member chlorapatite. (c) Relative enrichment map of Cl in the pegmatoid associated with the J-M Reef (ST_16_009), with stronger reds indicating higher Cl-content. Note the Cl-enriched apatite, amphibole and scapolite alteration rims and phases. (d) Quantified element map of Cl in the pegmatoid below the J-M Reef (ST_16_009). Cl-enrichment appears to be concentrated in the alteration rim of plagioclase to scapolite. (e) Quantified element map of Cl in the J-M Reef (ST_16_004) of approximately the same area as Fig. 2c, with a Cl-bearing apatite. (f) Quantified element map of Cl in ST_16_004. Note the Cl enrichment generally associated with apatite, plus alteration of olivine and clinopyroxene to serpentine. (g) Quantified element map of Cl in the pegmatoid vein below the S-poor J-M Reef (ST_16_011), with high Cl-areas associated with alteration of plagioclase and orthopyroxene. (h) Relative enrichment map of Cl in the massive sulfides (ST_16_005). High Cl contents are represented by blue-greens to yellows. The highest areas of enrichment are fractures in the thin section. Enrichment of Cl is seen in the clay grains (blue-green). Values for quantified maps in wt.%. Ap = apatite, Plg = plagioclase, Ol = olivine, Cpx = clinopyroxene, Opx = orthopyroxene, Mg-hb = magnesio-hornblende, Fe-hb = ferro-hornblende, Scap = scapolite, Serp = serpentine, Qtz = quartz, Slf = sulfides.

Figure 5. Halogen element abundance **(a, b)** and ratio plots **(c)** of all Stillwater Complex samples. Mineral separates shown with filled symbol and corresponding colour, and bulk signatures by open symbol. Greyscale symbols represent Rum Layered Intrusion halogen data from Parker et al. (2019). Mid Ocean Ridge Basalt and Ocean Island Basalt data (grey area) from Kendrick et al. (2012a, 2013, 2014). Seawater ratio line from Li (1982) and MORB

ratio line from Kendrick et al. (2012a, 2013, 2014). The ratio lines are based upon Cl, Br and I abundances of 18800 ppm 67 ppm and 60 ppb, respectively, for seawater (Li, 1982), and 329 ppm, 1 ppm and 15 ppb, respectively, for MORB (Kendrick et al., 2012a, 2013, 2014). The seawater point is from Li (1982). Subcontinental lithospheric mantle (SCLM) from Burgess et al. (2002). Hydration line from seawater indicates the directional influence on Br/Cl and I/Cl ratios as Cl is fractionated from Br and I during incorporation into hydrous mineral phases (from Svensen et al., 2001). Metasedimentary data (crosses) and unaltered greywacke (bold cross) are from Boneß et al. (1991).

Figure 6. (a) $^{130}Xe/^{36}Ar$ vs. $^{84}Kr/^{36}Ar$ isotopes plot and **(b)** $I/^{36}Ar$ and $^{130}Xe/^{36}Ar$ data from the 2018 set of Stillwater sample analysis. Mineral separates shown with solid symbol and corresponding colour of bulk signatures which are represented by open symbols. All data are from Stillwater Complex samples with the larger sample masses analysed in 2018 (**Table S2**). Mineral separates shown with solid symbol and corresponding colour of the bulk signatures represented by open symbols. (b) Reference values obtained from Matsuda and Nagao (1986), Staudacher and Allegre (1988), Holland and Ballentine (2006) and Kendrick et al. (2013). Greyscale symbols represent Rum Layered Intrusion halogen data from Parker et al. (2019).

This is the peer-reviewed, final accepted version for American Mineralogist, published by the Mineralogical Society of America.
The published version is subject to change. Cite as Authors (Year) Title. American Mineralogist, in press.
DOI: https://doi.org/10.2138/am-2022-7982. http://www.minsocam.org/

Table 1: *All NI-NGMS measurement data for the Stillwater Complex. Year is the year samples were analysed. Uncertainties are a standard error that account for propogation of analytical er*

Sample	Name	Type	Year	K (ppm)	Cl (ppm)	Br (ppb)	I (ppb)	K/Cl (wt.)	Br/Cl (wt. x10^{-3})	I/Cl (wt. x10^{-6})
ST_16_002	G chromite	Bulk	2018	91 ± 8	67.4 ± 4.6	1550 ± 110	13.2 ± 1.3	1.35 ± 0.12	23.0 ± 0.2	196 ± 7
ST_16_002	G chromite	Bulk	2018	96 ± 6	52.7 ± 3.6	1020 ± 70	8.4 ± 0.8	1.82 ± 0.12	19.3 ± 0.1	160 ± 5
ST_16_002	G chromite	Bulk	2019	nd	105 ± 8	893 ± 71	8.3 ± 1.3	nd	8.5 ± 0.1	79 ± 4
ST_16_002	G chromite	Bulk	2019	nd	nd	343 ± 107	2.2 ± 0.5	nd	nd	nd
ST_16_003	Pegmatite	Felsic fraction	2018	622 ± 35	26.7 ± 1.8	248 ± 19	11.9 ± 1.2	2.0 ± 0.3	9.3 ± 0.1	448 ± 16
ST_16_003	Pegmatite	Felsic fraction	2019	nd	5.7 ± 1.2	59 ± 17	3.6 ± 1.3	2.9 ± 3.8	10.4 ± 1.5	627 ± 74
ST_16_003	Pegmatite	Felsic fraction	2019	nd	nd	46 ± 7	1.9 ± 0.5	nd	nd	nd
ST_16_003	Pegmatite	Mafic fraction	2019	125 ± 17	61.6 ± 4.2	627 ± 45	12.5 ± 1.3	nd	10.2 ± 0.1	203 ± 7
ST_16_003	Pegmatite	Mafic fraction	2019	nd	nd	230 ± 61	6.1 ± 1	nd	nd	nd
ST_16_003	Pegmatite	Mafic fraction	2018	nd	26.3 ± 5.0	780 ± 202	10 ± 1.2	23.4 ± 1.3	29.7 ± 0.1	382 ± 24
ST_16_003	Pegmatite	Orthopyroxene	2019	157 ± 14	75.8 ± 5.3	265 ± 20	15.3 ± 1.6	2.07 ± 0.18	3.5 ± 0	202 ± 7
ST_16_003	Pegmatite	Orthopyroxene	2018	41 ± 11	25.7 ± 1.8	107 ± 8	10.9 ± 1.1	1.61 ± 0.44	4.2 ± 0.1	424 ± 15
ST_16_003	Pegmatite	Orthopyroxene	2018	87 ± 15	43.8 ± 3.0	334 ± 25	11.2 ± 1.1	1.98 ± 0.34	7.6 ± 0.1	257 ± 9
ST_16_004	Sulfide-rich J-M Reef	Bulk	2018	141 ± 12	405 ± 28	3820 ± 280	17.8 ± 1.8	0.35 ± 0.03	9.5 ± 0.1	44 ± 1
ST_16_004	Sulfide-rich J-M Reef	Bulk	2018	52 ± 11	641 ± 44	6420 ± 460	29.1 ± 2.9	0.08 ± 0.02	10.0 ± 0.1	45 ± 2
ST_16_004	Sulfide-rich J-M Reef	Bulk	2019	75 ± 36	5.7 ± 6.3	138 ± 215	0.8 ± 0.1	13.1 ± 7.5	24.2 ± 1.1	143 ± 67
ST_16_004	Sulfide-rich J-M Reef	Bulk	2019	56 ± 33	229 ± 16	1350 ± 100	8.2 ± 0.9	0.24 ± 0.15	5.9 ± 2.1	36 ± 1
ST_16_004	Sulfide-rich J-M Reef	Sulfide	2019	44 ± 13	9.5 ± 1.8	179 ± 46	5.4 ± 8.3	4.64 ± 1.45	18.7 ± 0.1	563 ± 246
ST_16_004	Sulfide-rich J-M Reef	Sulfide	2019	52 ± 16	23.7 ± 2.8	226 ± 35	2.4 ± 0.4	2.19 ± 0.68	9.5 ± 0.5	101 ± 6
ST_16_004	Sulfide-rich J-M Reef	Sulfide	2018	105 ± 12	22.5 ± 1.6	357 ± 27	4.8 ± 0.5	4.65 ± 0.54	15.9 ± 0.1	212 ± 8
ST_16_004	Sulfide-rich J-M Reef	Sulfide	2018	222 ± 24	49.7 ± 3.5	617 ± 47	5.9 ± 0.7	4.47 ± 0.49	12.4 ± 0.1	120 ± 4
ST_16_005	Massive sulfide	Bulk	2018	91 ± 8	10.7 ± 0.7	186 ± 14	1.9 ± 0.2	8.47 ± 0.75	17.4 ± 0.1	177 ± 7
ST_16_005	Massive sulfide	Bulk	2018	47 ± 6	4.4 ± 0.3	56 ± 4	1.5 ± 0.2	10.6 ± 1.9	12.8 ± 0.1	342 ± 13
ST_16_005	Massive sulfide	Bulk	2019	117 ± 78	27.1 ± 10.3	nd	nd	4.3 ± 3.0	nd	23 ± 6
ST_16_005	Massive sulfide	Bulk	2019	145 ± 34	nd	26 ± 9	0.7 ± 0.3	nd	nd	nd
ST_16_008	Sulfide-deficient J-M Reef	Felsic fraction	2018	822 ± 44	44.9 ± 3.1	359 ± 26	4.4 ± 0.5	18.3 ± 0.9	8.0 ± 0.1	nd
ST_16_008	Sulfide-deficient J-M Reef	Felsic fraction	2019	1280 ± 80	nd	103 ± 222	0.6 ± 0.4	nd	nd	nd
ST_16_008	Sulfide-deficient J-M Reef	Felsic fraction	2018	1020 ± 60	35.6 ± 4.6	206 ± 35	2.3 ± 0.4	2.68 ± 0.15	5.8 ± 0.1	65 ± 4
ST_16_008	Sulfide-deficient J-M Reef	Mafic fraction	2019	929 ± 51	346 ± 24	763 ± 55	9.0 ± 0.9	nd	2.2 ± 0.1	26 ± 1
ST_16_008	Sulfide-deficient J-M Reef	Mafic fraction	2019	506 ± 39	53.1 ± 5.1	213 ± 25	3.0 ± 0.4	9.53 ± 0.74	4.0 ± 0.1	56 ± 3
ST_16_008	Sulfide-deficient J-M Reef	Mafic fraction	2019	413 ± 36	46.5 ± 4.1	221 ± 23	3.4 ± 0.4	8.89 ± 0.77	4.8 ± 0.1	73 ± 3
ST_16_009	Pegmatoid	Felsic fraction	2019	997 ± 53	169 ± 12	2540 ± 180	25.6 ± 2.6	0.13 ± 0.01	15 ± 0.1	151 ± 5
ST_16_009	Pegmatoid	Felsic fraction	2019	1290 ± 80	10100 ± 700	360000 ± 26000	9160 ± 910	0.78 ± 0.05	35.3 ± 0.1	900 ± 31
ST_16_009	Pegmatoid	Felsic fraction	2018	1030 ± 60	6920 ± 480	187000 ± 13000	3220 ± 320	0.62 ± 0.04	27 ± 0.2	465 ± 16
ST_16_009	Pegmatoid	Mafic fraction	2018	1044 ± 57	5510 ± 380	128000 ± 9100	3000 ± 300	5.89 ± 0.32	23.3 ± 0.1	545 ± 19
ST_16_009	Pegmatoid	Mafic fraction	2018	1300 ± 70	13500 ± 930	239000 ± 17000	4460 ± 440	0.48 ± 0.03	17.6 ± 0.1	330 ± 11
ST_16_009	Pegmatoid	Mafic fraction	2019	2210 ± 140	2830 ± 200	23200 ± 1700	184 ± 18	1.62 ± 0.09	8.2 ± 0.1	65 ± 2
ST_16_009	Pegmatoid	Amphibole	2019	1870 ± 100	3030 ± 210	820 ± 60	16.5 ± 1.7	0.15 ± 0.01	0.3 ± 0.1	5 ± 1
ST_16_009	Pegmatoid	Amphibole	2018	1437 ± 78	3000 ± 200	770 ± 60	17.8 ± 1.9	0.19 ± 0.02	0.3 ± 0.1	6 ± 1
ST_16_009	Pegmatoid	Amphibole	2019	1400 ± 80	864 ± 59	620 ± 50	17.9 ± 1.9	0.10 ± 0.01	0.7 ± 0.1	21 ± 1
ST_16_011	Pegmatoid Vein	Felsic fraction	2019	4080 ± 220	17.9 ± 3.7	106 ± 30	1.5 ± 0.4	228 ± 12	5.9 ± 0.1	85 ± 7
ST_16_011	Pegmatoid Vein	Mafic fraction	2019	209 ± 30	871 ± 60	4370 ± 320	31.4 ± 3.2	0.24 ± 0.04	5.0 ± 0.1	36 ± 1
ST_16_011	Pegmatoid Vein	Bulk	2018	897 ± 48	684 ± 47	6580 ± 470	27 ± 2.7	1.31 ± 0.07	9.6 ± 0.1	40 ± 1
ST_16_011	Pegmatoid Vein	Bulk	2018	347 ± 20	742 ± 51	6600 ± 480	33.5 ± 3.3	0.47 ± 0.03	8.9 ± 0.1	45 ± 2

rror of the measurement, corrections, uncertainties in irradiation parameters, and sample mass.

FIGURE 1

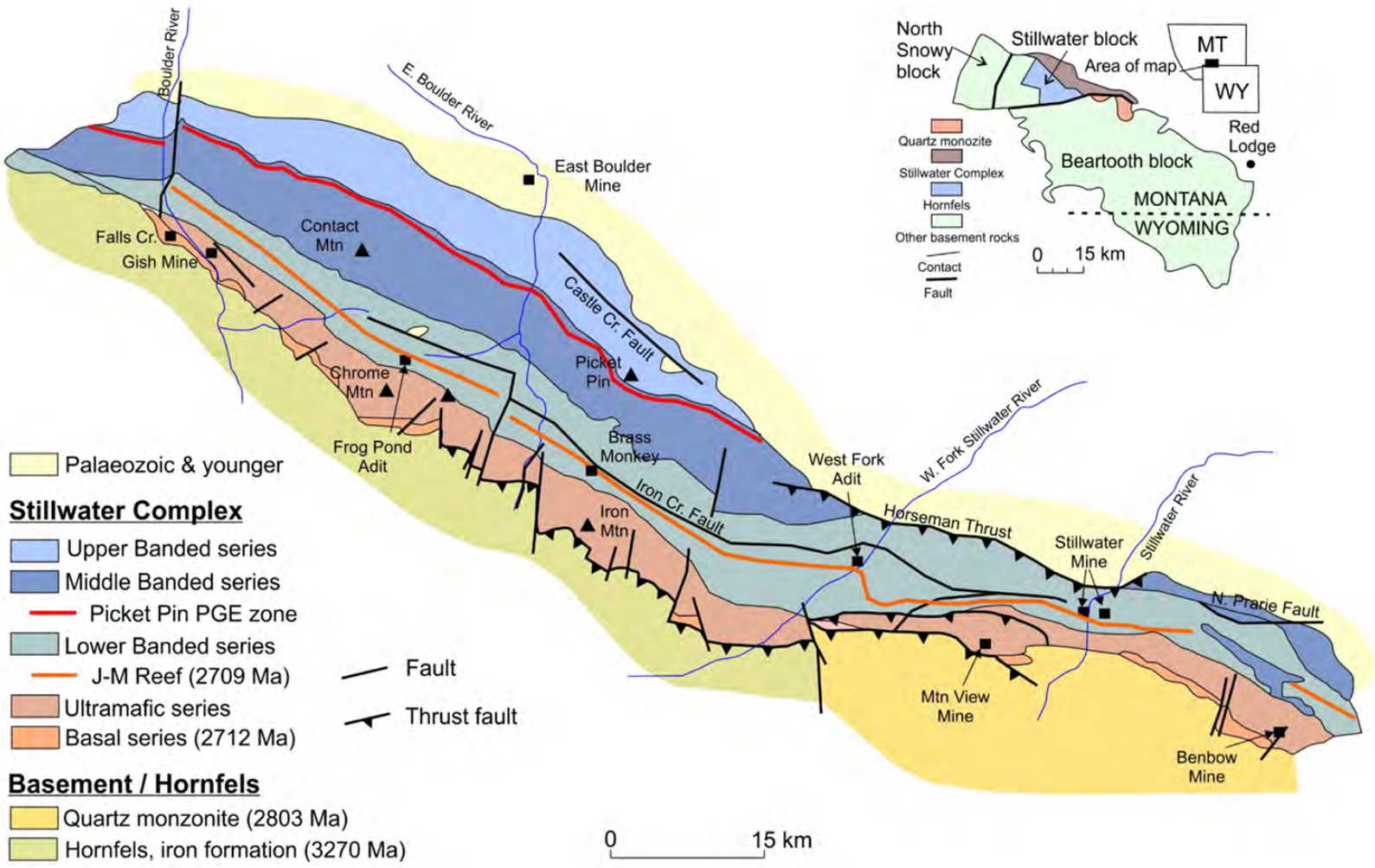
Boulder River
E. Boulder River
East Boulder Mine
Falls Cr.
Gish Mine
Contact Mtn
Castle Cr. Fault
Picket Pin
Chrome Mtn
Frog Pond Adit
Brass Monkey
Iron Cr. Fault
Iron Mtn
West Fork Adit
W. Fork Stillwater River
Horseman Thrust
Stillwater River
Stillwater Mine
N. Prarie Fault
Mtn View Mine
Benbow Mine
Palaeozoic & younger
Stillwater Complex
Upper Banded series
Middle Banded series
Picket Pin PGE zone
Lower Banded series
J-M Reef (2709 Ma)
Ultramafic series
Basal series (2712 Ma)
Fault
Thrust fault
Basement / Hornfels
Quartz monzonite (2803 Ma)
Hornfels, iron formation (3270 Ma)
0 15 km
North Snowy block
Stillwater block
Area of map
MT
WY
Red Lodge
Beartooth block
MONTANA
WYOMING
Quartz monozite
Stillwater Complex
Hornfels
Other basement rocks
Contact
Fault
0 15 km

FIGURE 2

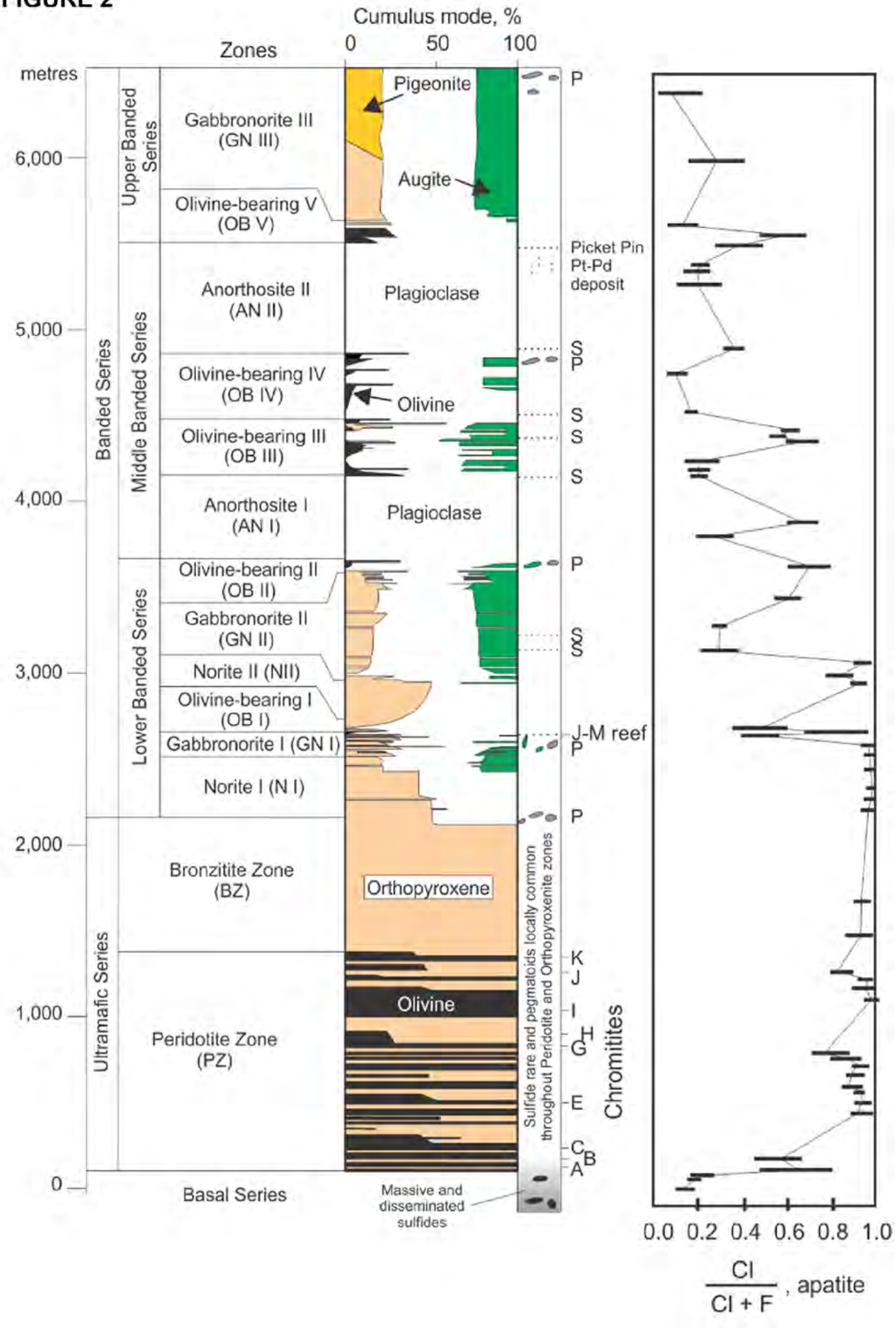
Cumulus mode, %
0
50
100
Zones
metres
6,000
5,000
4,000
3,000
2,000
1,000
0
Banded Series
Upper Banded Series
Middle Banded Series
Lower Banded Series
Ultramafic Series
Gabbronorite III (GN III)
Olivine-bearing V (OB V)
Anorthosite II (AN II)
Olivine-bearing IV (OB IV)
Olivine-bearing III (OB III)
Anorthosite I (AN I)
Olivine-bearing II (OB II)
Gabbronorite II (GN II)
Norite II (NII)
Olivine-bearing I (OB I)
Gabbronorite I (GN I)
Norite I (N I)
Bronzitite Zone (BZ)
Peridotite Zone (PZ)
Basal Series
Pigeonite
Augite
Plagioclase
Olivine
Plagioclase
Orthopyroxene
Olivine
Massive and disseminated sulfides
Sulfide rare and pegmatoids locally common throughout Peridotite and Orthopyroxenite zones
P
S
P
S
S
S
P
S
P
J-M reef
P
P
K
J
I
H
G
E
C
B
A
Picket Pin Pt-Pd deposit
Chromitites
0.0 0.2 0.4 0.6 0.8 1.0
Cl / (Cl + F), apatite

FIGURE 3

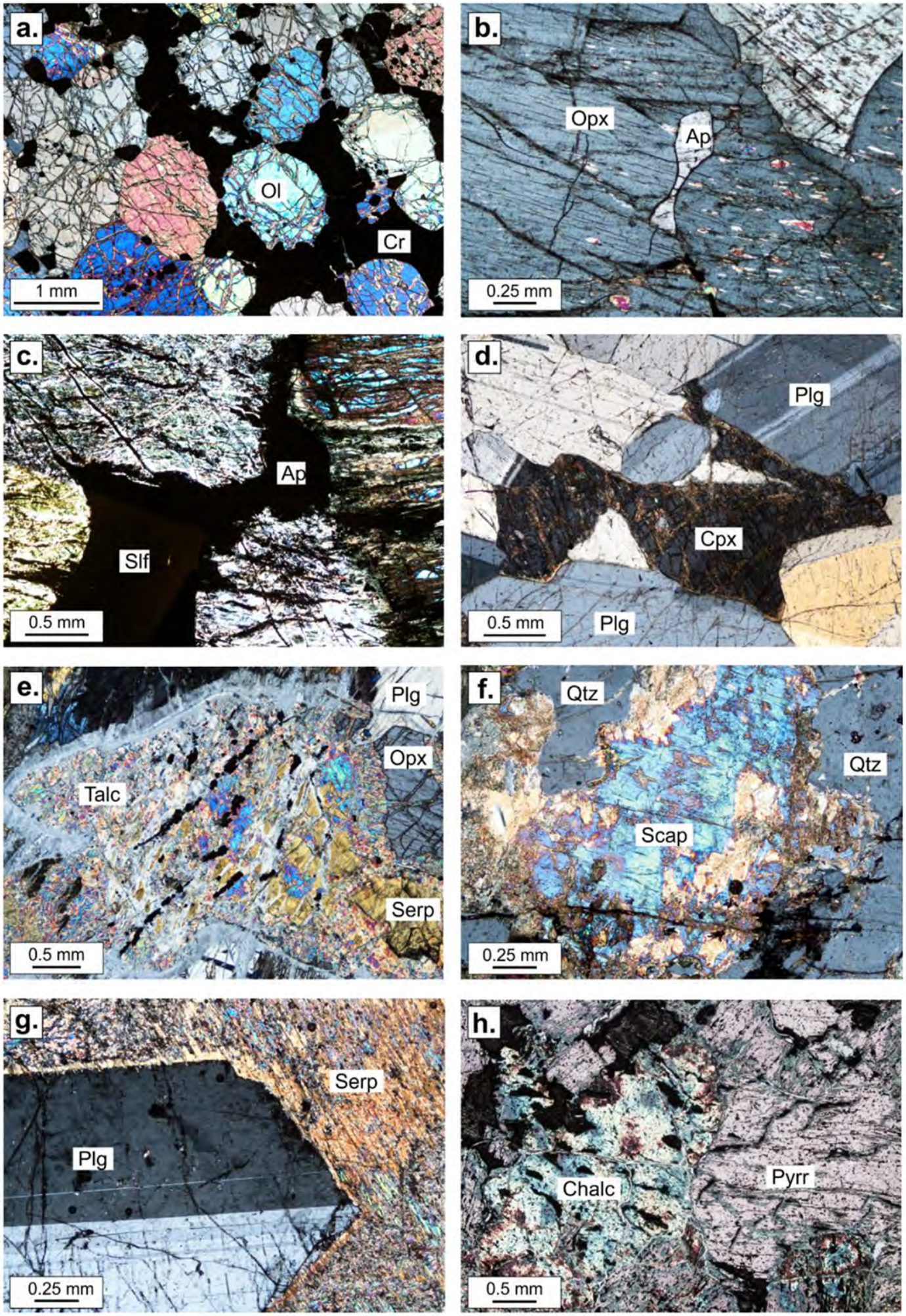
a.
Ol
Cr
1 mm
b.
Opx
Ap
0.25 mm
c.
Ap
Slf
0.5 mm
d.
Plg
Cpx
0.5 mm
Plg
e.
Plg
Opx
Talc
Serp
0.5 mm
f.
Qtz
Qtz
Scap
0.25 mm
g.
Serp
Plg
0.25 mm
h.
Chalc
Pyrr
0.5 mm

FIGURE 4

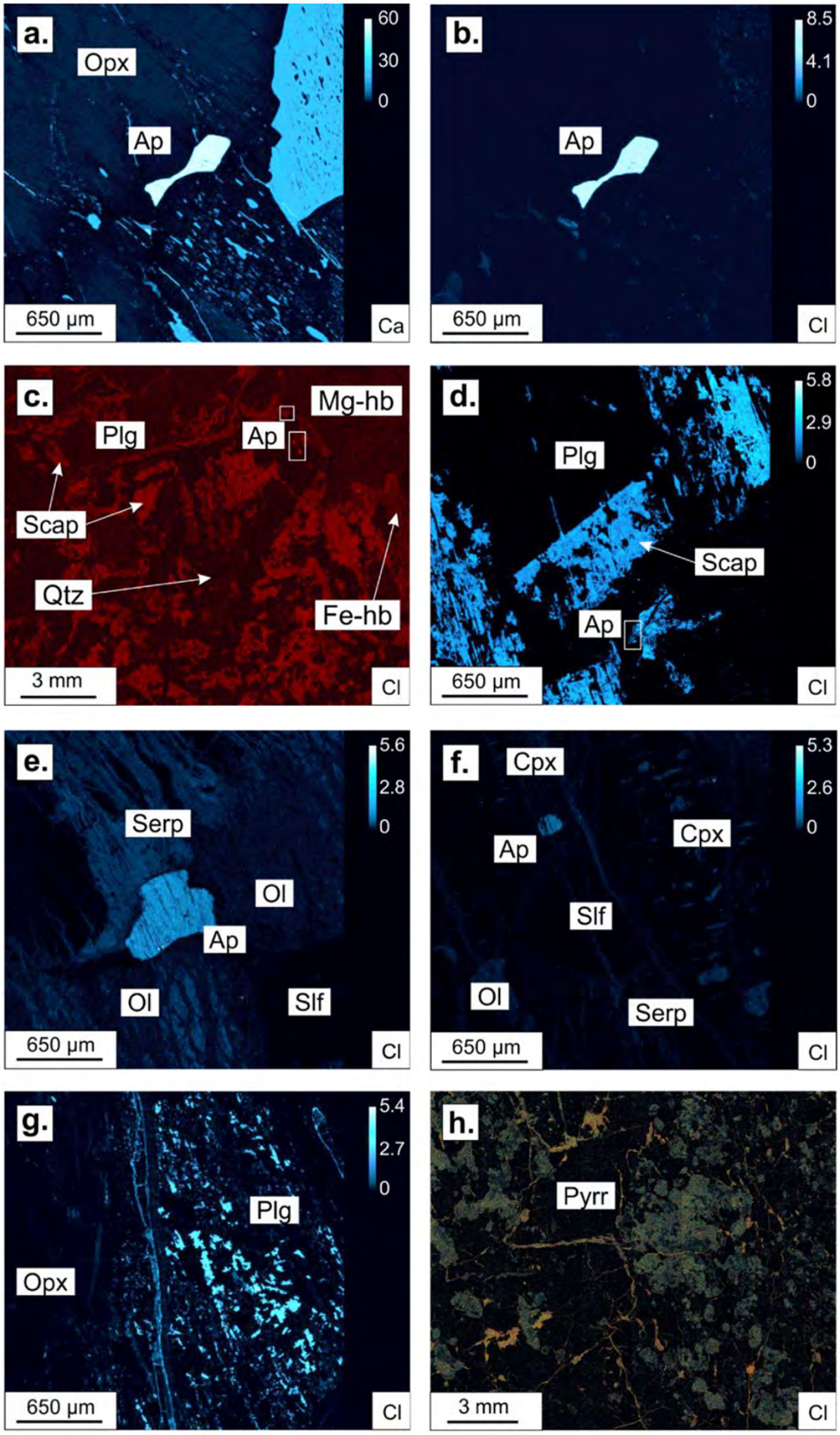
a.
Opx
Ap
60
30
0
650 µm
Ca
b.
Ap
8.5
4.1
0
650 µm
Cl
c.
Mg-hb
Plg
Ap
Scap
Qtz
Fe-hb
3 mm
Cl
d.
Plg
Scap
Ap
5.8
2.9
0
650 µm
Cl
e.
Serp
Ol
Ap
Ol
Slf
5.6
2.8
0
650 µm
Cl
f.
Cpx
Ap
Cpx
Slf
Ol
Serp
5.3
2.6
0
650 µm
Cl
g.
Plg
Opx
5.4
2.7
0
650 µm
Cl
h.
Pyrr
3 mm
Cl

FIGURE 5

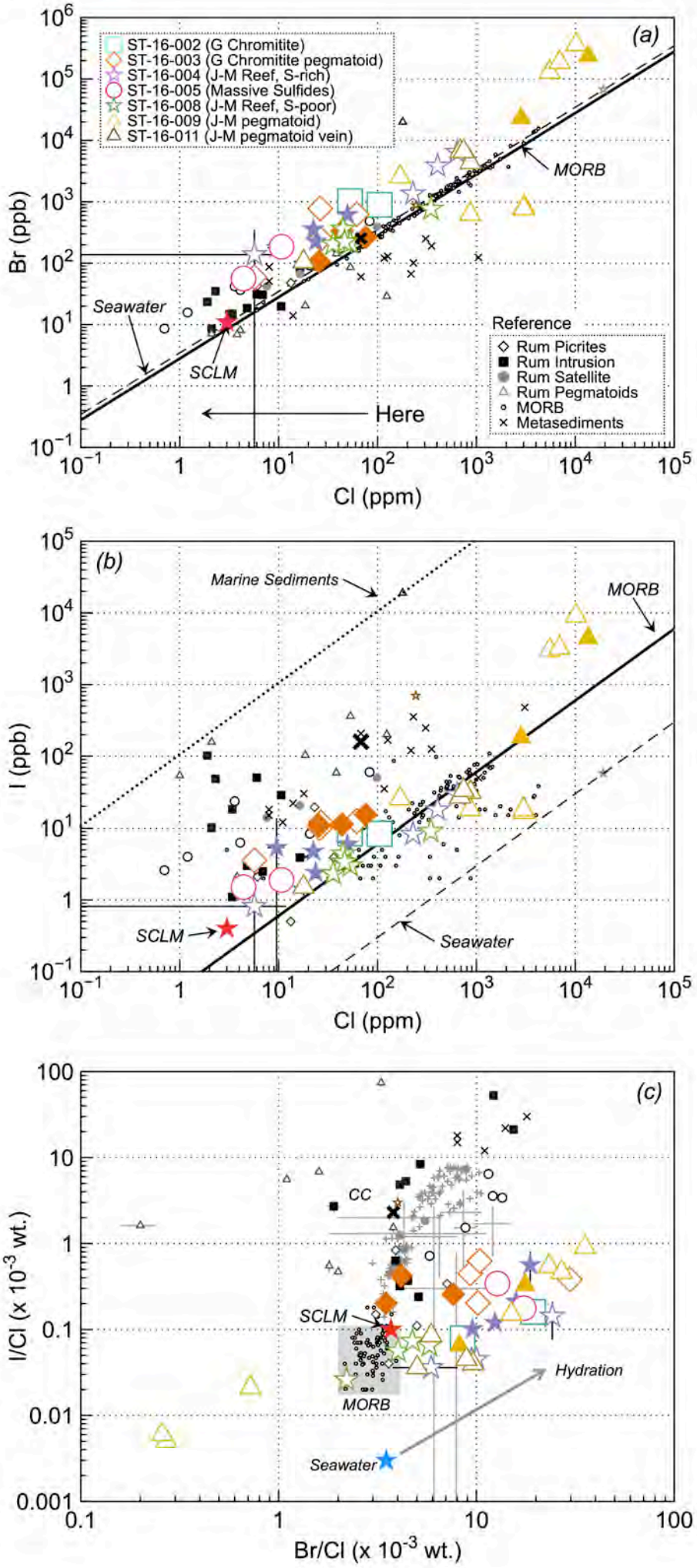
(a)
ST-16-002 (G Chromitite)
ST-16-003 (G Chromitite pegmatoid)
ST-16-004 (J-M Reef, S-rich)
ST-16-005 (Massive Sulfides)
ST-16-008 (J-M Reef, S-poor)
ST-16-009 (J-M pegmatoid)
ST-16-011 (J-M pegmatoid vein)
MORB
Seawater
SCLM
Here
Reference
Rum Picrites
Rum Intrusion
Rum Satellite
Rum Pegmatoids
MORB
Metasediments
Br (ppb)
Cl (ppm)
(b)
Marine Sediments
MORB
SCLM
Seawater
I (ppb)
Cl (ppm)
(c)
CC
SCLM
MORB
Hydration
Seawater
I/Cl (x 10-3 wt.)
Br/Cl (x 10-3 wt.)

FIGURE 6

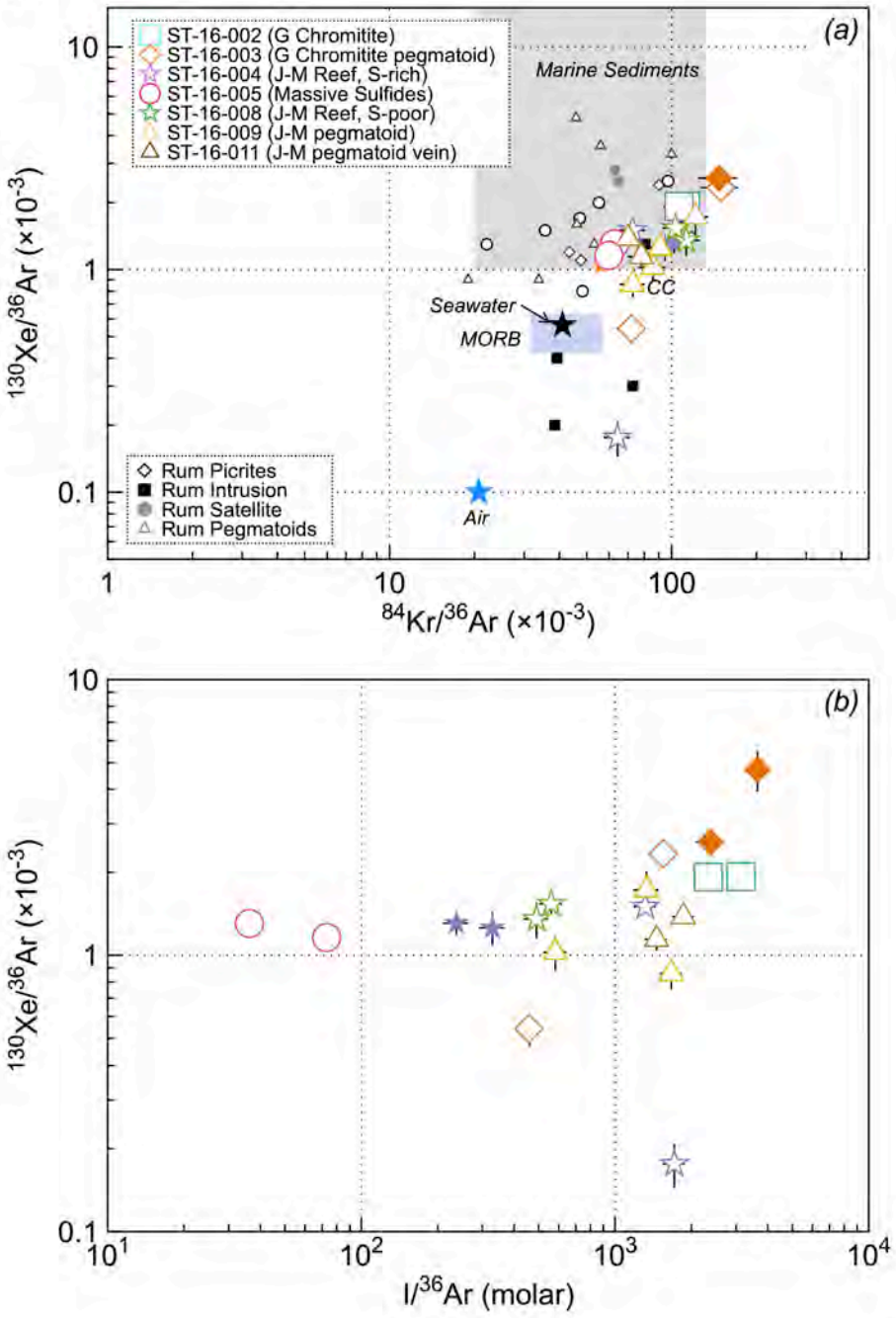
(a)
ST-16-002 (G Chromitite)
ST-16-003 (G Chromitite pegmatoid)
ST-16-004 (J-M Reef, S-rich)
ST-16-005 (Massive Sulfides)
ST-16-008 (J-M Reef, S-poor)
ST-16-009 (J-M pegmatoid)
ST-16-011 (J-M pegmatoid vein)
Marine Sediments
CC
Seawater
MORB
Air
Rum Picrites
Rum Intrusion
Rum Satellite
Rum Pegmatoids
$^{130}Xe/^{36}Ar$ (×10^{-3})
$^{84}Kr/^{36}Ar$ (×10^{-3})
(b)
$^{130}Xe/^{36}Ar$ (×10^{-3})
$I/^{36}Ar$ (molar)